Primate-specific BTN3A2 protects against SARS-CoV-2 infection by interacting with and reducing ACE2

Ling Xu[1,2,3,*], Dandan Yu[1,2,3], Min Xu[1,2], Yamin Liu[2,5], Lu-Xiu Yang[1], Qing-Cui Zou[3], Xiao-Li Feng[3], Ming-Hua Li[3], Nengyin Sheng[2,5,*], Yong-Gang Yao[1,2,3,4,*]

[1] Key Laboratory of Animal Models and Human Disease Mechanisms of the Chinese Academy of Sciences & Yunnan Province and KIZ/CUHK Joint Laboratory of Bioresources and Molecular Research in Common Diseases, Kunming Institute of Zoology, Chinese Academy of Sciences, Kunming, 650204, China

[2] Kunming College of Life Science, University of Chinese Academy of Sciences, Kunming, 650204, China

[3] Kunming National High-Level Biosafety Research Center for Non-Human Primates, Center for Biosafety Mega-Science, Kunming Institute of Zoology, Chinese Academy of Sciences, Kunming, 650107, China

[4] National Resource Center for Non-Human Primates, National Research Facility for Phenotypic & Genetic Analysis of Model Animals (Primate Facility), Kunming Institute of Zoology, Chinese Academy of Sciences, Kunming, 650107, China

[5] State Key Laboratory of Genetic Resources and Evolution, Key Laboratory of Animal Models and Human Disease Mechanisms of Yunnan Province, Kunming Institute of Zoology, Chinese Academy of Sciences, Kunming, 650201, China

[*] Corresponding authors: Dr. Yong-Gang Yao, E-mail: yaoyg@mail.kiz.ac.cn or Dr. Ling Xu, E-mail: xuling0502@mail.kiz.ac.cn or Dr. Nengyin Sheng, E-mail: shengnengyin@mail.kiz.ac.cn

Abstract

Coronavirus disease 2019 (COVID-19) is an immune-related disorder caused by severe acute respiratory syndrome coronavirus 2 (SARS-CoV-2). SARS-CoV-2 invades cells via the entry receptor angiotensin-converting enzyme 2 (ACE2). While several attachment factors and co-receptors for SARS-CoV-2 have been identified, the complete pathogenesis of the virus remains to be determined. Unraveling the molecular mechanisms governing SARS-CoV-2 interactions with host cells is crucial for the formulation of effective prophylactic measures and the advancement of COVID-19 therapeutics. Here, we identified butyrophilin subfamily 3 member A2 (BTN3A2) as a potent inhibitor of SARS-CoV-2 infection. The mRNA level of *BTN3A2* was correlated with COVID-19 severity. Upon re-analysis of a human lung single-cell RNA sequencing dataset, *BTN3A2* expression was predominantly identified in epithelial cells. Moreover, this expression was elevated in pathological epithelial cells from COVID-19 patients and co-occurred with ACE2 expression in the same cellular subtypes in the lung. Additionally, BTN3A2 primarily targeted the early stage of the viral life cycle by inhibiting SARS-CoV-2 attachment through direct interactions with the receptor-binding domain (RBD) of the Spike protein and ACE2. Furthermore, BTN3A2 inhibited ACE2-mediated SARS-CoV-2 infection by reducing ACE2 *in vitro* and in a BTN3A2 transgenic mouse model. These results reveal a key role of BTN3A2 in the fight against COVID-19 and broaden our understanding of the pathobiology of SARS-CoV-2 infection. Identifying potential monoclonal antibodies

that target BTN3A2 may facilitate disruption of SARS-CoV-2 infection, providing a therapeutic avenue for COVID-19.

Keywords: BTN3A2, ACE2, Spike protein, SARS-CoV-2, COVID-19

Introduction

The emergence of coronavirus disease 2019 (COVID-19), caused by severe acute respiratory syndrome coronavirus 2 (SARS-CoV-2), precipitated a global pandemic with persistent pathological sequelae (1,2). According to the World Health Organization, the pandemic resulted in more than 6.9 million deaths in recent years (3), posing a significant threat to global health and economic security (4). SARS-CoV-2 induces extensive damage to multiple organ systems via an overactive host immune response. To date, most research efforts have focused on the development of pan-sarbecovirus vaccines and neutralizing antibodies (5). However, the pathogenesis of COVID-19, especially key molecular events in the early stage of viral infection, remains incompletely understood. This knowledge gap contributes to the limited availability of effective and specific antiviral agents against SARS-CoV-2 (6). Therefore, further efforts are required to clarify host-virus interactions and viral pathogenesis and thus identify candidate targets for the prevention and treatment of SARS-CoV-2 infection.

Receptor binding constitutes a critical step in viral invasion (7). In the case of SARS-CoV-2, the Spike protein, specifically the receptor-binding domain (RBD) in S1 subunit, mediates recognition of the host ACE2 receptor to facilitate viral entry (8-12). Mutations in the Spike protein, particularly in the RBD, can lead to immune evasion, reduced efficacy of existing vaccines, and escape from neutralizing antibodies, as exemplified by the global spread of the Omicron variants (13,14). Consequently, identifying broad-spectrum antiviral targets and additional candidates

that are effective against different viral variants has become a critical objective in combating the COVID-19 pandemic. Viral host receptors such as ACE2, which is indispensable for SARS-CoV-2 cellular entry, present attractive candidates for intervention (15). ACE2 is a transmembrane carboxypeptidase with broad substrate specificity, including angiotensin II, which is essential for viral entry (10). Importantly, as ACE2 is a host factor, its expression is less likely to be affected by viral mutations. This suggests that therapeutic approaches aimed at modulating ACE2 expression may be effective against multiple SARS-CoV-2 variants (16). Hence, the exploration of drugs or targets that either directly or indirectly affect ACE2 to modulate SARS-CoV-2 infection represents a viable strategy for investigation.

Situated in the juxta-telomeric region of the MHC-I locus, the butyrophilin subfamily 3 (*BTN3*) is a member of the immunoglobulin transmembrane superfamily, initially noted for its role in lactation and milk production (17,18). The three primary members of the BTN3A family, BTN3A1, BTN3A2, and BTN3A3, share similar extracellular domains. BTN3A1 and BTN3A3 contain an intracellular B30.2 domain that is absent in BTN3A2. The *BTN3A2* is a primate-specific gene that likely evolved during primate lineage development (19). Members of the BTN3 family members are expressed in most human immune cell subsets and are known to participate in immunomodulatory functions (20). BTN3A2, in particular, has been implicated in the evolutionary and development of the primate brain (21) and is associated with various psychological disorders (19,22,23). While historically not associated this family with antiviral properties, recent studies have identified BTN3A3 as a restriction factor

against Ebola virus replicons (24) and as a key barrier to avian influenza A virus spillover into humans (25). In the context of SARS-CoV-2, there has been an observed up-regulation in the mRNA expression levels of *BTN3A2* and *BTN3A3* in Calu-3 cells, along with other related genes (26). Despite these observations, the precise mechanisms underlying this regulation remain to be clarified.

In this study, we assessed the potential role of BTN3A2 as a key host factor in combating SARS-CoV-2 infection. Based on publicly available datasets and newly obtained data, we observed an up-regulation of *BTN3A2* mRNA expression in COVID-19 patients and non-human primates (NHPs). Using cellular and animal models of SARS-CoV-2 infection, we also established that BTN3A2 competed with the ACE2 via directly interacting with the SARS-CoV-2 Spike RBD, thereby reducing ACE2 receptor expression and ACE2-mediated SARS-CoV-2 entry. This study identified BTN3A2 as a host factor against SARS-CoV-2 infection, providing a basis for the development of potential small molecule inhibitors targeting BTN3A2 for the treatment of COVID-19.

Results

BTN3A2 was altered in COVID-19 patients and SARS-CoV-2-infected NHPs

We first analyzed *BTN3A2* mRNA expression in peripheral blood mononuclear cells (PBMCs) from COVID-19 patients based on published transcriptomic data (27) to examine potential relevance between *BTN3A2* and SARS-CoV-2 infection. Results showed a significantly increased *BTN3A2* mRNA level in COVID-19 patients (Non-

ICU COVID-19) compared to non-COVID-19 patients (ICU and Non-ICU) (P=5.3×10^{-4}, Fig. 1A). However, in critically ill COVID-19 patients (ICU COVID-19), *BTN3A2* mRNA expression was significantly reduced relative to Non-COVID-19 patients (P=1.42×10^{-6}, Fig. 1A). In monocytic-myeloid-derived suppressor cells (M-MDSCs) from COVID-19 patients with different disease severities and stages (28), no marked differences in *BTN3A2* mRNA expression were found between the healthy controls and asymptomatic patients or healthy controls and convalescent patients, but expression was significantly reduced in patients with severe COVID-19 relative to healthy controls (P=3.6×10^{-3}, Fig. 1A). Re-analyses of scRNA-seq data of PBMCs, B cells, T cells (CD4^{+} T, CD8^{+} T, and other T cells), and natural killer (NK) cells (29) also showed an up-regulation of *BTN3A2* mRNA expression in most cell types in COVID-19 patients compared to healthy controls.

The *BTN3A2* gene is expressed in various myeloid and immune cells and plays an important role in the immune response (30). However, the functional implications of elevated *BTN3A2* expression in the lungs, which are the primary target organs for SARS-CoV-2, remain to be elucidated. Hence, we first explored the expression of *BTN3A2* in healthy human lung tissues using available GTEx data (31). Results indicated that the lungs had the second highest *BTN3A2* expression among 30 tested tissues (Fig. S1A). Among the different cell types in the lung tissue, alveolar type 1 and 2 cells, together with alveolar macrophages, showed relatively high *BTN3A2* expression (Fig. S1B). Further analysis of the scRNA-seq datasets of COVID-19 patient lungs (32) showed that epithelial cells had the highest *BTN3A2* expression

(Fig. 1B), which are the primary target cells of SARS-CoV-2 (33).

We further explored *BTN3A2* expression patterns in NHPs challenged with SARS-CoV-2, given their heightened resemblance to humans in the cellular identities and frequencies of putative viral target cells (8,34). Among 15 tissues tested in rhesus monkeys (35), lung tissues showed the highest expression level of *BTN3A2* (Fig. S1C). Immunohistochemical analysis also showed that BTN3A2 was constitutively expressed in the healthy lung tissues of rhesus monkeys (Fig. S1D). We quantified the changes in *BTN3A2* mRNA expression in rhesus and cynomolgus monkeys (*Macaca fascicularis*) using RT-qPCR. Results indicated that *BTN3A2* mRNA levels were significantly up-regulated in PBMCs and lung tissues at 7 dpi with SARS-CoV-2 in rhesus macaques (Fig. 1C) and cynomolgus monkeys (Fig. 1D). Similar *BTN3A2* mRNA expression patterns have also been observed in the transcriptomic data of rhesus monkeys with early SARS-CoV-2 infection (35) (Fig. S1E). Collectively, these results indicate that *BTN3A2* is up-regulated in COVID-19 patients and NHPs infected with SARS-CoV-2.

BTN3A2 acted as a potent SARS-CoV-2 restriction factor

BTN3A2, a member of the immunoglobulin superfamily, is implicated in diverse cellular processes (17). BTN3A2 contains both full-length BTN3A2 (BTN3A2-L) and truncated BTN3A2 (BTN3A2-S), as identified in our previous report (19). To evaluate the potential role of BTN3A2 in inhibiting SARS-CoV-2, we first ectopically expressed the BTN3A family members (BTN3A1, BTN3A3, and BTN3A2) in ACE2-

A549 cells (Fig. S2A), which were then infected with SARS-CoV-2. Both BTN3A2 isoforms significantly inhibited SARS-CoV-2 viral copy numbers, whereas BTN3A1 and BTN3A3 had no apparent inhibitory effect (Fig. 2A). Compared to a higher multiplicity of infection (MOI), overexpression of BTN3A2 in ACE2-HEK293T had a more potent inhibitory effect on lower infectious titers (Fig. 2B and Fig. S2B). The Huh7 cell line, which endogenously expresses ACE2 and is naturally susceptible to SARS-CoV-2 (36), was used to validate the above results. Overexpressing BTN3A2 in Huh7 cells (Fig. S2C) significantly reduced viral copies of the SARS-CoV-2 prototype and BA.2 variant in cytoplasm and culture supernatant (Fig. 2C). Similar inhibitory effects were observed using pseudotyped virus, which is a heterologous virus with Spike protein (37) in Calu-3 cells overexpressing BTN3A2 isoforms (Fig. 1D). Interestingly, pre-incubation of soluble BTN3A2-L and BTN3A2-S proteins with Calu-3 cells blocked viral entry into cells, with a dose-dependent inhibitory effect (Fig. 2E).

To further test the potential role of endogenous BTN3A2 in controlling SARS-CoV-2 infection, we depleted BTN3A2 expression in Huh7 cells using CRISPR-Cas9 gene editing, as described in our previous study (38), with two individual sgRNAs (sgBTN3A2-1 and sgBTN3A2-3; Fig. S2D). BTN3A2 knockout cells were more susceptible to authentic and pseudovirus SARS-CoV-2 than cells without BTN3A2 knockout (Fig. 2F-G). Thus, these findings suggest that BTN3A2 can restrict SARS-CoV-2 infection.

BTN3A2 directly interacted with Spike protein at RBD

Next, we characterized the effects of BTN3A2 on specific steps of the viral replication cycle. Huh7 cells were transduced with a two-lentivirus system that included a construct expressing BTN3A2 under a tet-inducible promoter and a doxycycline-dependent reverse tetracycline-controlled trans-activator (rtTA). This system allowed precise control of BTN3A2 expression levels in the transduced Huh7 cells through doxycycline treatment (Fig. S3A). Initially, we assessed whether BTN3A2 inhibits SARS-CoV-2 attachment to the cell surface. Our data showed that SARS-CoV-2 viral copies were significantly reduced in Dox-induced cells (Dox+) overexpressing BTN3A2-L and BTN3A2-S but not in the corresponding control cells (Dox−) when cells were incubated with SARS-CoV-2 for viral attachment at 4 °C for 1 h (Fig. 3A). We switched the cells to 37 °C for 30 min to enable the internalization of bound SARS-CoV-2, followed by trypsin digestion of uninternalized virus, to explore the effects of BTN3A2 expression on SARS-CoV-2 entry. Similar SARS-CoV-2 viral copy loads were observed in cells under different treatments, suggesting that overexpression of BTN3A2 may not impact viral entry into cells (Fig. 3B). To assess whether BTN3A2 interacts with the SARS-CoV-2 Spike protein, an envelope protein essential for host cell binding and entry (39), we conducted a co-immunoprecipitation assay. Both BTN3A2 isoforms were co-immunoprecipitated with the Spike protein in the HEK293T cells (Fig. 3C). Of note, BTN3A2-L interacted with the Spike S1 subunit but not the S2 subunit (Fig. 3D), as confirmed by biolayer interferometry analysis (KD=92.7±0.111 nM) (Fig. 3E). The S1 subunit, which

contains the RBD, is both an inducer of dominant neutralizing antibodies (nAbs) in the host and a key antigenic target for vaccine development (40-42). Subsequent co-immunoprecipitation assays confirmed that BTN3A2-L interacted with the Spike protein RBD from multiple SARS-CoV-2 variants, including α, γ, δ, BA.1, BA.2, BA.2.12, and BA.5 (Fig. 3F). These findings establish BTN3A2 as a novel cellular binding partner for the SARS-CoV-2 Spike protein specifically at the RBD.

BTN3A2 competed with ACE2 to bind to RBD

Although several host receptors for SARS-CoV-2 have been identified, only ACE2 interacts with the Spike protein via the RBD (43). Thus, we tested whether BTN3A2 isoforms interact with ACE2, thereby modulating ACE2 and Spike protein interactions during viral entry and replication. Biolayer interferometry analysis revealed an affinity between BTN3A2-L and ACE2 (KD=92.7±0.359 nM) (Fig. 4A), as confirmed by co-immunoprecipitation of BTN3A2-L (His-tagged) with ACE2 in HEK293T cells (Fig. 4B-C), thus indicating a direct association between BTN3A2-L and ACE2.

As both ACE2 and BTN3A2 interacted with the Spike protein via its RBD, we further investigated whether BTN3A2 competes with ACE2 for Spike S1 subunit binding. Based on competitive ELISA, the interaction between ACE2 and SARS-CoV-2 Spike was measured in the presence of recombinant BTN3A2-L protein (Fig. 4D). Results showed that Spike-ACE2 binding was greatly diminished under increasing BTN3A2-L concentrations in a dose-dependent manner. At high BTN3A2-

L concentrations, the affinity between BTN3A2-L and the ACE2-Spike S1 subunit was similar to that of the BTN3A2-L-Spike S1 subunit (Fig. 4E). Co-immunoprecipitation assays demonstrated a decrease in the expression levels of RBD and ACE2 under the ectopic expression of BTN3A2-L in HEK293T cells (Fig. 4F). These findings suggest that BTN3A2 interacts with the Spike through RBD binding, and ACE2 and BTN3A2 compete for binding to the Spike protein.

BTN3A2 inhibited ACE2 expression

We next explored the potential role of the interactions among BTN3A2, ACE2, and Spike protein in the context of COVID-19 pathology. We first compared the tissue distribution patterns of BTN3A2 and ACE2. Re-analyses of a large-cohort RNA-seq dataset of GTEx human tissues (31) showed that *BTN3A2* mRNA expression exhibited a reverse correlation with *ACE2* in the lungs and gastrointestinal tract (small intestine) (Fig. S4A), which are major targets of SARS-CoV-2 infection. A similar pattern was also observed in lung tissues and cell lines with or without SARS-CoV-2 infection (44) (Fig. S4B). We further compared *BTN3A2* expression patterns relative to those of *ACE2* in different lung cell types using scRNA-seq data from COVID-19 patients (32). Our results indicated that, following SARS-CoV-2 infection, *ACE2* expression was moderately elevated in the lung epithelial cells of COVID-19 patients. In contrast, *BTN3A2* expression was substantially up-regulated in the same cell type (Fig. 5A). To further determine whether BTN3A2 affects ACE2 expression, we assessed whether stable expression of *BTN3A2* in Huh7 cells altered the expression of

ACE2 mRNA. Our results indicated that *ACE2* mRNA expression was significantly decreased in Huh7 cells stably expressing BTN3A2-L and BTN3A2-S (Fig. 5B). Consistently, total ACE2 protein expression was markedly decreased in HEK293T cells overexpressing both BTN3A2-L and ACE2 compared to cells overexpressing ACE2 only (Fig. 5C). The inhibitory effects of BTN3A2-L on ACE2 expression were dose-dependent (Fig. 5D). Knockout of BTN3A2 in Huh7 cells led to a significant increase in both *ACE2* mRNA (Fig. 5E) and protein levels (Fig. 5F). Using flow cytometry, we further assessed whether BTN3A2 alters ACE2 expression on the cell surface. Notably, ACE2 expression on the cell surface was significantly decreased in Calu-3 cells overexpressing BTN3A2 isoforms, while BTN3A2 knockdown increased the surface level of ACE2 (Fig. 5G-H). Similar results were observed for the Huh7 cell line (Fig. S4C-D), indicating that BTN3A2 inhibits ACE2 expression *in vitro*.

As *BTN3A2* is a primate-specific gene (19,25), we used BTN3A2-tg mice to further characterize the level of ACE2 *in vivo*. WT C57BL/6J mice were used as a control. Mice were intranasally infected with AAV-hACE2 (AAV-hACE2 group) or AAV-EGFP (AAV-EGFP (control) group). Immunoblot analysis showed that EGFP levels were similar between the BTN3A2-tg and WT C57BL/6J mice (WT control) (Fig. 5I), indicating effective viral vector-mediated gene expression. Consistent with the cellular assays and inhibitory effects of BTN3A2 on ACE2 expression, our results further showed that the ACE2 protein level was significantly lower in BTN3A2-tg mice relative to WT C57BL/6J mice (Fig. 5I). The AAV vectors achieved efficient EGFP and ACE2 expression in the lung tissues of WT mice at 14 dpi with AAV (Fig.

5J). Conversely, ACE2 was barely detected in the lung tissues of BTN3A2-tg mice (Fig. 5J). Collectively, these results suggest that BTN3A2 suppression of ACE2 also occurs *in vivo*.

BTN3A2 suppressed SARS-CoV-2 infection by reducing ACE2

We further evaluated whether the suppression of ACE2 expression by BTN3A2 is responsible for BTN3A2-mediated SARS-CoV-2 restriction. We intranasally injected AAV9-hACE2 (AAV carrying the human *ACE2* gene) in WT C57BL/6J and BTN3A2 transgenic (BTN3A2-tg) heterozygous mice and observed for two weeks, followed by SARS-CoV-2 challenge and sacrifice for tissue collection at 3 dpi (Fig. 6A). Quantitative analysis of viral loads, specifically targeting the nucleoprotein gene (*N*) and envelope gene (*E*), revealed a 3–6-fold decrease in lung tissue viral concentrations in BTN3A2-tg mice compared to their WT counterparts (Fig. 6B). Of the seven infected WT C57BL/6J mice examined, five exhibited detectable levels of viral subgenomic RNA in their lung tissues, including the subgenomic E (sgE) gene, a marker of infectious virus (45). In contrast, none of the six BTN3A2-tg mice showed detectable levels of sgE gene. Further immunohistochemical staining of the SARS-CoV-2 nucleoprotein (N) showed a consistent reduction in viral protein levels in the lung tissues of BTN3A2-tg mice compared to the infected WT C57BL/6J mice (Fig. 6C). Moreover, histological analysis showed that the lung tissues of the SARS-CoV-2 infected BTN3A2-tg mice had milder damage, including the widening, fusion, and increased solidity of the pulmonary septa, compared to the infected WT C57BL/6J

mice (Fig. 6D), suggesting a protective role of BTN3A2 in counteracting SARS-CoV-2 infection. Similarly, we observed consistent and effective expression of hACE2 in the lung tissues of the WT group, while the protein level of ACE2 was greatly reduced in the lung tissues of the BTN3A2-tg mice, as expected (Fig. 6E). This pattern was further validated by immunohistochemical analysis of lung tissues from both groups: ACE2 was consistently and highly expressed in the upper and lower respiratory tract of WT mice (Fig. 6F) but was barely detected in the respiratory tract of BTN3A2-tg mice. Collectively, these results suggest that BTN3A2 can restrict SARS-CoV-2 by suppressing ACE2-mediated viral entry *in vivo*.

Discussion

Understanding the pathobiology of SARS-CoV-2 infection is essential for developing effective treatments. Various studies have examined the host immune response in relation to SARS-CoV-2 infection (46-48). Specifically, the balanced regulation of interferon signaling and immune response has been shown to substantially influence disease severity and outcomes of COVID-19 (49). In the current study, we identified BTN3A2 as a novel factor involved in the defense against SARS-CoV-2 infection. Notably, BTN3A2 was up-regulated upon SARS-CoV-2 infection and directly interacted with the RBD of the Spike protein. This interaction was confirmed through both cell-free binding assays utilizing recombinant proteins and co-immunoprecipitation assays conducted in cellular environments. This led to competitive interference with the interaction between ACE2 and the RBD of the Spike

protein, as reported previously (8,50). Given that BTN3A2 is a single transmembrane protein localized to the cellular membrane (51), it is plausible that a complex between BTN3A2 and the Spike protein may effectively obstruct the binding of the Spike protein to ACE2 on the cellular surface. Remarkably, BTN3A2-S, which lacks a transmembrane domain, demonstrated greater efficacy than BTN3A2-L in inhibiting the attachment of the Spike protein to the cellular surface, thereby reducing SARS-CoV-2 infection. We hypothesize that secreted BTN3A2-S (19) may possess enhanced inhibitory effects against SARS-CoV-2 Spike binding to ACE2, akin to the function of neutralizing antibodies. Investigating the structural characteristics and molecular dynamics of the BTN3A2-Spike protein complex could offer substantial insights for the engineering of short peptides that retain the full competitive capacity of BTN3A2 in challenging ACE2 for Spike protein binding.

Prior genome-wide Mendelian randomization analyses identified ACE2 as a promising target candidate for COVID-19 drug development (15). Reducing ACE2 expression is also considered a potentially efficacious host-directed prophylaxis for protection against SARS-CoV-2 infection (16). Beyond the competitive effects of BTN3A2 on ACE2-Spike binding, our study demonstrated that BTN3A2 interacted with ACE2, leading to a further decrease in ACE2 expression. Overexpression of BTN3A2 led to a reduction in *ACE2* mRNA and protein levels, which further inhibited ACE2-mediated SARS-CoV-2 infection, both *in vitro* and *in vivo*. While the exact mechanism by which BTN3A2 regulates ACE2 expression remains to be determined, the apparent dual role of BTN3A2 in regulating ACE2 expression and

function is consistent with the concept that targeting universal host factors essential for viral replication offers advantages in terms of broad-spectrum effectiveness and reduced drug resistance (52,53).

The ongoing COVID-19 pandemic, coupled with the emergence of new SARS-CoV-2 variants, necessitates the development of novel broad-spectrum vaccines and antiviral therapies (52,53). Recent studies have identified several potential targets for SARS-CoV-2 intervention, including the transcriptional regulator BRD2 (48), aryl hydrocarbon receptor (AhR) (6), and host cysteine-aspartic protease caspase-6 (6), for which specific compounds have been characterized. Given the observed protective effects of BTN3A2 against SARS-CoV-2 infection, we speculate that BTN3A2 may be a viable host factor candidate with broad antiviral potential. Indeed, pre-incubation of soluble BTN3A2 protein with host cells resulted in decreased viral entry. Notably, interactions between BTN3A2 and the Spike protein RBD of various SARS-CoV-2 variants of concern (VOCs) (e.g., prototype, α, γ, δ, and omicron) remained largely stable despite the rich diversity and evolution of viral sequences. These findings suggest the anti-coronavirus activity of BTN3A2 may be both conserved and efficacious across multiple SARS-CoV-2 VOCs.

The primate-specific *BTN3A2* gene (19,25) is highly expressed in the brain. Thus, it may have a role in the development of long COVID and brain fog, conditions characterized by a multitude of persistent neurological symptoms that last for months after SARS-CoV-2 infection (54). Currently, the pathophysiological mechanisms associated with neurological symptoms derived from SARS-CoV-2 infection remain

to be elucidated (55). We recently showed that the S2 subunit of the SARS-CoV-2 Spike protein modulates γ-secretase and enhances Aβ production, which may contribute to the neurological alterations observed in COVID-19 patients (56). Respiratory infection with SARS-CoV-2 can elicit neuroinflammation and dysfunction in neural cells and myelin (57). Modulation of the immune environment within the central nervous system, particularly in scenarios where neuroinflammation is triggered by inflammation in the respiratory system, may influence the neuroprotective and neuroplastic functions of specific immune cell populations, including γδ T cells (58), following COVID-19 (55). Therefore, given the broad immune cell expression of BTN3A2 (30) and its involvement in γδ T cell regulation (59), determining the roles of BTN3A2 in T cell-mediated immune responses, neuroinflammation, and long COVID-19 would be worthwhile.

In conclusion, we identified BTN3A2 as a novel host factor with protective effects against SARS-CoV-2 infection. Thus, BTN3A2 holds considerable potential as a therapeutic drug for mitigating the impact of SARS-CoV-2 VOCs. However, subsequent research is warranted to explore its potential role in the occurrence of neurological symptoms, commonly referred to as “brain fog”, in COVID-19 patients.

Materials and Methods

Viral strains and cells

The SARS-CoV-2 prototype was kindly provided by the Guangdong Provincial Center for Disease Control and Prevention (Guangdong, China), as described in our

previous studies (60-62). The virus was amplified in Vero-E6 cells and median tissue culture infective dose ($TCID_{50}$) was used to assess viral infectivity. The viral sequence is accessible from the China National Microbiology Data Center (NMDC, Accession No. NMDCN0000HUI). The SARS-CoV-2 variant BA.2 was isolated from a patient in Yunnan Provincial Infectious Disease Hospital and its sequence is accessible at NMDC (Accession No. NMDC60046377) (37). Virions from the fourth passage were used in all experiments. The VSV-G pseudotyped viruses (G*ΔG-VSV-Rluc), containing prototype and variant BA.1, were kindly provided by Dr. Yong-Tang Zheng at Kunming Institute of Zoology (KIZ), Chinese Academy of Sciences (CAS).

The HEK293T, Huh7, A549, and Vero E6 cells were obtained from the Kunming Cell Bank, KIZ, and were grown in Dulbecco's Modified Eagle Medium (DMEM, high glucose) supplemented with 10% fetal bovine serum (FBS) and 1% penicillin/streptomycin. The Calu-3 cells were purchased from Procell Life Science & Technology Co., Ltd. Cells were cultured in Minimum Essential Medium (MEM; Gibco, USA) supplemented with 10% FBS (Gibco, USA), 1% MEM non-essential acids (Gibco, USA), 1% sodium pyruvate (100 mM, Gibco, USA), and 1% antibiotics. All cells were cultured at 37 °C in a humidified atmosphere of 5% CO_2.

Plasmid construction and transfection

Two transcripts of human *BTN3A2* were cloned into Flag-tagged pCMV-3Tag-8, as described in our previous report (19). Briefly, the coding region of *BTN3A2* was sub-cloned into a pCMV-3Tag-8-His vector using the same primers and sub-cloned

into pCMV-HA using EcoR I/Xho I. The expression vector for the SARS-CoV-2 Spike protein (pCMV3-2019-nCoV-Spike (S1+S2)-long) was purchased from Sino Biological (VG40589-UT, China). The expression vector for ACE2 was purchased from Miaolinbio (pEnCMV-ACE2 (human)-3×FLAG, P16698, China). The expression vectors for the Spike S1 (S-S1) and Spike S2 subunits (S-S2) were reported in our previous study (56). The expression vector for the prototype RBD (pEnCMV-RBD (SARS-CoV-2)-3×FLAG) was purchased from Miaolinbio (P15640, China), while the expression vectors for the SARS-CoV-2 variant RBDs of the S1 subunit (including α, γ, δ, BA.1, BA.2, BA.2.12, and BA.5) were kindly provided by Dr. Jinghua Yan at Institute of Microbiology, CAS. All primers used to construct plasmids are listed in Supplementary Table S1. Each construct was verified by direct Sanger sequencing.

The HEK239T cells were transfected using Lipofectamine™ 3000 (L3000008, Invitrogen, USA) following the manufacturer's protocols. In brief, the cells were cultured in 6-well plates and grown to 70% confluence. The cells in each well were then transfected with 270 μL of solution containing 2.5 μg of plasmid DNA, 250 μL of Opti-MEM medium (31985-070, Gibco-BRL,USA), and 12.5 μL of Lipofectamine™ 3000. Cells were incubated with the transfection mixture for 6 h at 37 °C in a humidified atmosphere of 5% CO_2, with the medium changed to growth medium for 42 h before harvest.

Generation of genetically modified cell lines

Individual single-guide RNAs (sgRNAs) (sgBTN3A2 #1: TGTTCTCTCCCTTGGCGTTGCTCCACTGTA; sgBTN3A2 #3: ATCATGAGAGGCGGCTCCGGGGAGGGTGTATC) targeting the candidate gene were cloned into linearized lentiCRISPRv2 (#52961, Addgene, USA). Lipofectamine™ 3000 transfection reagent in Opti-MEM medium was used to co-transfect HEK293T cells with psPAX2 (#12260, Addgene, USA), pMD2.G (# 12259, Addgene, USA), and indicated individual sgRNA constructs at a ratio of 2:1:3, in accordance with the manufacturer's instructions. Transfection medium was replaced with viral production medium at 6 h after transfection. The supernatant was collected and filtered using a 0.45 μm filter (Millipore, USA) at 72 h after transfection. Huh7 and Calu-3 cells were transduced with 1 mL of harvested lentiviral stock with polybrene (1 mg/mL) for 24 h. The cells were then switched to 2 mL of fresh medium and puromycin (1 μg/mL) to select for successfully transduced cells. The lentiviral particle of sgRNA (lentiCRISPRv2 vector) was used as a control.

A lentiviral expression system for ACE2 was established using the pLenti-CMV-ACE2-Flag plasmid (Public Protein/Plasmid Library, China) in HEK293T cells. For lentiviral infection, both HEK293T and A549 cells were seeded in 6-well plates at a density of 4×10^5 cells/well. After 12 h of culture, the culture medium was replaced by infection mixture containing 1 mL of culture medium with 1 μg of polybrene (H8761, Solarbio, China) and 1 mL of viral supernatants. Subsequently, the culture medium was replaced with 2 mL of fresh medium containing puromycin (1 μg/mL) to select for successfully transduced cells.

The coding region sequences of two BTN3A2 isoforms (BTN3A2 long isoform, BTN3A2-L; BTN3A2 short isoform, BTN3A2-S) were sub-cloned from pCMV-HA-BTN3A2-L and pCMV-HA-BTN3A2-S expression vectors into the pLVX-tight-puro vector (632162, Clontech, USA) (Supplementary Table S1). The TETon system was combined with a separate lentiviral compatible vector containing the reverse tetracycline-controlled transactivator Advance (rtTA Advance) (632162, Clontech, USA). Lentiviral particles corresponding to either TETon-BTN3A2 or rtTA Advance were generated using the above procedures. Huh7 and Calu-3 cells were transduced with the TETon-BTN3A2 (pLVX-Vector, pLVX-BTN3A2-L, and pLVX-BTN3A2-S) and rtTA Advance lentiviral particles (each 1 mL) in the presence of polybrene (1 mg/mL) for 48 h. The culture medium was replaced with 2 mL of fresh medium and incubated for an additional 24 h. Cells were subsequently selected using G418 (250 ng/mL) and puromycin (1 μg/mL) for a minimum of two weeks.

Western blotting and immunoprecipitation

Western blotting and immunoprecipitation were performed using the same procedures described in our previous study (63). In brief, cells were lysed on ice in RIPA lysis buffer (P0013, Beyotime Institute of Biotechnology, China) and centrifuged at 12 000 *g* and 4 °C for 5 min to harvest cell lysates. Protein concentration was determined using a BCA Protein Assay Kit (P0012, Beyotime Institute of Biotechnology, China). Bovine serum albumin (BSA; P0007, Beyotime Institute of Biotechnology, China) was used as the protein standard. Cell lysates (20

μg of total protein/sample) were separated by 12% sodium dodecyl-sulfate polyacrylamide gel electrophoresis (SDS-PAGE), before transfer to polyvinylidene fluoride (PVDF) membranes (IPVH00010, Roche Diagnostics, China) using standard procedures. The membranes were then blocked with 5% non-fat dry milk in Tris-buffered saline (#9997, Cell Signaling Technology, USA) with 0.1% Tween 20 (P1379, Sigma, USA) (TBST) at room temperature for 2 h. Membranes were incubated with primary antibodies against His (1:5 000), HA (1:5 000), Flag (1:5 000), ACE2 (1:1 000), BTN3A2 (1:1 000), Spike (1:1 000), and Tubulin (1:10 000) overnight at 4 °C, respectively. The membranes were washed three times (5 min each) with TBST and incubated with TBST-conjugated anti-mouse or anti-rabbit secondary antibody (1:10 000) for 1 h at room temperature. After washing with TBST three times, the proteins on the membranes were detected by enhanced chemiluminescence reagents (WBKLS0500, Millipore, USA).

For immunoprecipitation, appropriate antibodies were incubated with protein G-agarose beads (15920010, Life Technologies, USA) to form a complex for 2 h at room temperature. Cells were lysed with RIPA lysis buffer on ice for 1 h, followed by centrifugation at 12 000 *g* for 10 min at 4 °C. The lysates were then immunoprecipitated with the complex at 4 °C overnight, followed by four washes with RIPA lysis buffer and resuspension in loading sample buffer for SDS-PAGE.

Flow cytometry

To measure the cell surface expression level of ACE2, indicated cells were

washed with phosphate-buffered saline (PBS) and stained with mouse anti-ACE2 (# 66699-1-Ig, Proteintech, China) at a 1:50 dilution for 30 min at 4 °C. The cells were then washed twice and resuspended in 1×PBS containing secondary antibody (AF647-labeled donkey anti-goat immunoglobulin G (IgG), # A31571, Invitrogen, USA) at a 1:500 dilution. After 30 min of incubation at 4 °C, the cells were washed twice and resuspended in 1×PBS before flow cytometry analysis using FACSCelesta (BD Biosciences, USA). Data were analyzed using FlowJo software.

Re-analysis of RNA-sequencing (RNA-seq) datasets

RNA-seq data of blood leukocytes collected from 26 hospitalized non-COVID-19 patients and 100 COVID-19 patients with different degrees of disease severity were obtained from the Gene Expression OmniBus (GEO, www.ncbi.nlm.nih.gov/geo/, accession number GSE157103) (27). Of these individuals, 16 non-COVID-19 patients and 50 COVID-19 patients were admitted to the intensive care unit (ICU). The RNA-seq dataset of monocytic-myeloid-derived suppressor cells (M-MDSCs) from 12 COVID-19 patients (four severe, four asymptomatic, and four convalescent) and four controls were downloaded from the GEO database (accession number GSE178824) (28). Raw RNA-seq data of 15 tissues from three rhesus macaques (*Macaca mulatta*) infected with SARS-CoV-2 and one control were downloaded from the China National Center for Bioinformation (https://www.cncb.ac.cn/) (accession number CRA004025) (35). The raw sequencing reads were first cleaned using Trimmomatic v0.33 (64), then mapped to the rhesus macaque reference genome (Mmul_10,

https://www.ncbi.nlm.nih.gov/datasets/genome/GCF_003339765.1/) using STAR v2.7.3a (65). Gene expression quantification was conducted with RSEM v1.3.1 (66).

Single-cell RNA-seq (scRNA-seq) data of peripheral blood from five healthy donors and 27 COVID-19 patients were downloaded from https://atlas.fredhutch.org/fredhutch/covid/dataset/merged (67). ScRNA-seq data of lung tissues from seven controls and 19 COVID-19 patients were downloaded from https://singlecell.broadinstitute.org/single_cell/study/SCP1219/columbia-university-nyp-covid-19-lung-atlas (32). The expression levels of *BTN3A2* and *ACE2* in bulk non-disease human tissues and single cells were obtained from the GTEx Portal (https://www.gtexportal.org/) (31,68). RNA-seq data of mock (n=3) and SARS-CoV-2 (n=3)-infected lung-derived Calu-3 cells, primary human lung epithelial cells (NHBE) and lung biopsies from healthy controls (n=2) and postmortem COVID-19 patients (n=2) were obtained from the GEO database (accession number GSE147507) (69,70). Raw counts were normalized using DESeq2 (71) and batch effects among samples were removed using the removeBatchEffect function from limma (72). For bulk RNA-seq data, the *BTN3A2* expression levels were compared between different groups using two-sided t-tests. For scRNA-seq data, the *BTN3A2* expression levels were compared between different groups for each cell type using two-sided Wilcox rank sum tests. Expressional correlations between two genes were calculated using Pearson's correlation.

Animals and tissues

Left lobe lung tissue from rhesus macaques (*n*=6) (73) and cynomolgus macaques (*n*=8) (74) infected with SARS-CoV-2 were obtained from the tissue bank of the Animal Biosafety Level 3 (ABSL-3) facility at KIZ, CAS. Lung tissues from healthy rhesus macaques (*n*=5) and cynomolgus macaques (*n*=6) were purchased from the National Resource Center for Non-Human Primates, KIZ.

C57BL/6J wild-type (WT) mice were obtained from the Experimental Animal Core Facility of KIZ, CAS. Humanized *BTN3A2* knock-in mice were generated using CRISPR/Cas9 on a C57BL6/J background by inserting the coding sequence of the human *BTN3A2* gene (Transcript ID: ENST00000356386.6) into the *Hipp11* (*H11*) locus. The BTN3A2 transgenic (BTN3A2-tg) mice were created by GemPharmatech (Nanjing, China). Both male and female mice (4 weeks) were used for the experiments. All mice were genotyped by PCR with genomic DNA prepared from tail tips using primer pair 5'-CAGCAAAACCTGGCTGTGGATC-3'/5'-CGTAGATGTACTGCCAAGTAGG-3'.

Animal models for SARS-CoV-2 infection

To evaluate whether adeno-associated virus (AAV) exhibits good efficiency for overexpressing exogenous protein in mouse tissues, we infected four age-matched C57BL/6J (*n*=2) and BTN3A2-tg (*n*=2) mice with enhanced green fluorescent protein (EGFP)-expressing AAV (AAV-EGFP) (PackGene Biotech, Guangzhou, China). Briefly, mice were intranasally infected with AAV-EGFP (PackGene Biotech, Guangzhou, China) at a total volume of 30 μL containing 2×10^{12} viral genome copies.

The AAV-EGFP-infected mice were sacrificed at 14 days post-infection (dpi) with AAV.

Human ACE2 (hACE2) was overexpressed using hACE2-expressing AAV (AAV-hACE2) in C57BL/6J (*n*=9) mice and BTN3A2-tg mice (*n*=8). In brief, mice were intranasally infected with AAV-hACE2 (PackGene Biotech, Guangzhou, China) at a total volume of 30 μL containing 2×10^{12} genome copies. The C57BL/6J (*n*=7) and BTN3A2-tg (*n*=6) mice were monitored daily until SARS-CoV-2 infection at 14 dpi with AAV-hACE2. After anesthetization with isoflurane (RWD Life Science, China), the mice were intranasally infected with a total volume of 30 μL containing 1×10^{5} $TCID_{50}$ of SARS-CoV-2 variant BA.2. All infected animals were housed at the ABSL-3 facility on a 12 h light/dark cycle, with free access to food and water. All animals were sacrificed at 3 dpi. The remaining C57BL/6J (*n*=2) and BTN3A2-tg (*n*=2) mice with AAV-hACE2 infection but without SARS-CoV-2 infection were assigned as the control group and sacrificed at 14 dpi with AAV.

Tissue samples were collected from all animals after euthanasia and stored in a −80 °C freezer (for quantification of mRNA and protein levels) or in 4% paraformaldehyde (PFA; for histological analysis and immunochemistry) until use.

All animal experiments were approved by the Institutional Animal Care and Use Committee of KIZ, CAS (Approval No: IACUC-RE-2023-03-004). All experiments involving live SARS-CoV-2 were conducted in the ABSL-3 facility at KIZ, CAS (Assurance No.: KIZP3-XMZR-2021-23 and KIZP3-XMZR-2023-04).

Measurement of viral RNAs

RNA copies per mL (cell RNA) or per μg (lung samples) were determined by quantitative real-time polymerase chain reaction (RT-qPCR), as described in our previous study (61). Briefly, total RNA was extracted from 200 μL of indicated cell supernatants using a High Pure Viral RNA Kit (Roche, Germany). The extracted RNA was eluted in 50 μL of elution buffer. TRIzol Reagent (Thermo Fisher Scientific, USA) was used for total RNA isolation from cells and homogenized tissues. Viral RNA copies were detected using a THUNDERBIRD Probe One-Step qRT-PCR Kit (TOYOBO, Japan). A total of 25 μL reaction solution, containing 8.7 μL of extracted RNA from indicated cell supernatant or 1 μg of total RNA from cells or lung tissue samples, was prepared for RT-qPCR analysis (61). The Applied Biosystems 7500 Real-Time PCR system was used for RT-qPCR analysis with the following thermal cycle conditions: 10 min at 50 °C for reverse transcription, 60 s at 95 °C, followed by 40 cycles at 95 °C for 15 s and 60 °C for 45 s. In each run, serial dilutions of the SARS-CoV-2 RNA reference standard (National Institute of Metrology, China) were used in parallel to calculate copy numbers in each sample.

Pathological analysis

The lungs of SARS-CoV-2-infected mice were fixed in 4% PFA for 7 days, processed in paraffin (Leica EG1160, Germany), sectioned to 3-4 μm thickness (Leica RM2255, Germany), and stained with hematoxylin and eosin (H&E), as described in our previous study (62). The slices were imaged using a Nikon Eclipse E100

microscope (Japan) and were evaluated in a blinded manner by two pathologists. Immunohistochemical analysis of lung tissue was performed based on previously described procedures (62,75). In brief, each section was baked at 65 °C for 30 min, followed by deparaffinization using xylene and subsequent hydration with decreasing concentrations of ethanol (100% to 75%). Heat-induced antigen retrieval was performed using sodium citrate buffer (pH 6.0). Endogenous peroxidase was blocked with 3% hydrogen peroxide for 25 min, and non-specific binding was blocked with 3% BSA for 30 min at room temperature. Specimens were incubated overnight at 4 °C with rabbit anti-SARS-CoV-2 nucleocapsid protein (Cell Signaling Technology, USA, #26369, 1:200), mouse anti-ACE2 (Cell Signaling Technology, USA, #74512, 1:100), mouse anti-GFP (Santa Cruz Biotechnology, USA, #sc-99961:2000), and mouse anti-BTN3A2 antibodies (ORIGENE, USA, #CF500730, 1:50), respectively. The slices were incubated with mouse IgG1 kappa isotype control (Thermo Fisher Scientific, USA, #14-4714-82) as a negative control for antigen staining. After washing with PBS with 0.1% Tween 20 three times, the lung slices were incubated with anti-rabbit IgG (Servicebio, China, # GB111738) or anti-mouse IgG secondary antibody (Servicebio, China, # GB111739) for 50 min at room temperature and visualized with 3,3'-diaminobenzidine tetrahydrochloride (DAB). The slices were counterstained with hematoxylin, dehydrated and mounted on a slide, and imaged under an Olympus OlyVIA microscope (Japan).

Enzyme-linked immunosorbent assay (ELISA) competition assays

Spike S1-Fc (Sino Biological, China, 40591-V02h, 6.25 ng/mL) was mixed with ACE2-Fc (Sino Biological, China, 10108-H02H, 50 ng/mL) or Human IgG-Fc (Sino Biological, China, 10702-HNAH, 50 ng/mL) at 4 °C overnight. The mixture was then added with a series of concentrations (0, 6.25, 12.5, 25, 50 ng/mL) of BTN3A2-His (Sino Biological, China, 13515-H08H). These sample series were transferred to a plate pre-coated with the spike glycoprotein S1-RBD from SARS-CoV-2 (Elabscience, China, E-EL-E605). After 2 h of incubation, the plate was washed by wash buffer three times. Avidin-horseradish peroxidase (HRP) conjugate was successively added to each microplate well and incubated at 4 °C for 30 min. The free components were then removed by washing and substrate solution was added to each well. Only those wells containing SARS-CoV-2 S1-RBD, biotinylated detection antibody, and Avidin-HRP conjugate appeared blue. The enzyme-substrate reaction was terminated by the addition of stop solution according to the manufacturer's instructions. Optical density was measured using a BioTek Synergy HT microplate reader (BioTek, USA).

Bio-layer interferometry (BLI) assay

The BLI assays were performed using the Octet RED96 system (ForteBio, Germany). Briefly, ACE2-Fc protein (10 μg/mL) was captured on AR2G Biosensors (ForteBio, Germany, # 18-5095) and incubated with a series of concentrations of BTN3A2-His (62.5, 250, 1 000, and 2 000 nM). The BLI assays were performed via four steps: (i) ACE2-Fc protein loading onto AR2G Biosensors (360s); (ii) baseline; (iii) association

of BTN3A2-His to determine Kon (association rate constant) (360 s); and (iv) dissociation of BTN3A2-His to determine Kdis (dissociation constant) (360 s). The baseline and dissociation steps were performed in SD buffer (pH 7.4 PBS, 0.05% Tween 20, 0.01% BSA) and biosensor drifting was corrected by background subtraction. Background wavelength shifts were measured in the reference biosensors only loaded with ACE2-Fc in SD buffer. All steps were conducted in a shaker (1 000 rpm, 30 °C). The data were analyzed and fitted in a 1:1 binding model using Octet data analysis software (ForteBio v9.0). The same procedure was used to determine whether BTN3A2 binds to Spike S1. Briefly, BTN3A2-His protein (10 μg/mL) was captured on AR2G Biosensors and incubated with Spike S1-Fc (125, 250, 500, and 1 000 nM) at various concentrations.

Acknowledgments

We thank Dr. Yu-Lin Yao (Wuhan institute of Virology, CAS) and Dr. Yong Wu (Affiliated Wuhan Mental Health Center, Jianghan University) for technical discussions. This study was supported by the National Natural Science Foundation of China (U1902215, 32070569 and 32371017), Key Project of the CAS “Light of West China” Program (to D.Y. and L.X.), and Yunnan Province (202305AH340006, 202305AH340007).

Author contributions

L.X., N.S., Y-G.Y. conceptualized and supervised the study. L.X., D.Y., M.X., Y.L., Y-X.L., Q-C.Z., X-L.F., M-H.L. performed the experiments. L.X., D.Y. and M.X. analyzed the data. L.X., D.Y., M.X., N.S. and Y-G.Y. wrote the manuscript. All authors have given approval to the final version of the manuscript.

Competing interests

The authors declare that they have no competing interests.

References

1. Wiersinga WJ, Rhodes A, Cheng AC, Peacock SJ, Prescott HC, Pathophysiology, transmission, diagnosis, and treatment of coronavirus disease 2019 (COVID-19): a review. *JAMA* **324**: 782-793 (2020).
2. Mehandru S, Merad M, Pathological sequelae of long-haul COVID. *Nat. Immunol.* **23**: 194-202 (2022).
3. Organization WH, 2023. "Coronavirus disease (COVID-19) pandemic." World Health Organization, November 21, 2023. https://www.who.int/news-room/fact-sheets/detail/coronavirus-disease-(covid-19).
4. Parotto M, Gyöngyösi M, Howe K, Myatra SN, Ranzani O, Shankar-Hari M, Herridge MS, Post-acute sequelae of COVID-19: understanding and addressing the burden of multisystem manifestations. *Lancet Respir. Med.* **11**: 739-754 (2023).
5. Barouch DH, Covid-19 Vaccines - Immunity, Variants, Boosters. *N. Engl. J. Med.* **387**: 1011-1020 (2022).
6. Shi J, Du T, Wang J, Tang C, Lei M, Yu W, Yang Y, Ma Y, Huang P, Chen H, Wang X, Sun J, Wang H, Zhang Y, Luo F, Huang Q, Li B, Lu S, Hu Y, Peng X, Aryl hydrocarbon receptor is a proviral host factor and a candidate pan-SARS-CoV-2 therapeutic target. *Sci. Adv.* **9**: eadf0211 (2023).
7. Lu G, Wang Q, Gao GF, Bat-to-human: spike features determining 'host jump' of coronaviruses SARS-CoV, MERS-CoV, and beyond. *Trends Microbiol.* **23**: 468-478 (2015).
8. Ziegler CGK, Allon SJ, Nyquist SK, Mbano IM, Miao VN, Tzouanas CN, Cao Y, Yousif AS, Bals J, Hauser BM, Feldman J, Muus C, Wadsworth MH, 2nd, Kazer SW, Hughes TK, Doran B, Gatter GJ, Vukovic M, Taliaferro F, Mead BE, Guo Z, Wang JP, Gras D, Plaisant M, Ansari M, Angelidis I, Adler H, Sucre JMS, Taylor CJ, Lin B, Waghray A, Mitsialis V, Dwyer DF, Buchheit KM, Boyce JA, Barrett NA, Laidlaw TM, Carroll SL, Colonna L, Tkachev V, Peterson CW, Yu

A, Zheng HB, Gideon HP, Winchell CG, Lin PL, Bingle CD, Snapper SB, Kropski JA, Theis FJ, Schiller HB, Zaragosi LE, Barbry P, Leslie A, Kiem HP, Flynn JL, Fortune SM, Berger B, Finberg RW, Kean LS, Garber M, Schmidt AG, Lingwood D, Shalek AK, Ordovas-Montanes J, SARS-CoV-2 receptor ACE2 is an interferon-stimulated gene in human airway epithelial cells and is detected in specific cell subsets across tissues. *Cell* **181**: 1016-1035.e1019 (2020).

9. Taft JM, Weber CR, Gao B, Ehling RA, Han J, Frei L, Metcalfe SW, Overath MD, Yermanos A, Kelton W, Reddy ST, Deep mutational learning predicts ACE2 binding and antibody escape to combinatorial mutations in the SARS-CoV-2 receptor-binding domain. *Cell* **185**: 4008-4022.e4014 (2022).

10. Zhou P, Yang XL, Wang XG, Hu B, Zhang L, Zhang W, Si HR, Zhu Y, Li B, Huang CL, Chen HD, Chen J, Luo Y, Guo H, Jiang RD, Liu MQ, Chen Y, Shen XR, Wang X, Zheng XS, Zhao K, Chen QJ, Deng F, Liu LL, Yan B, Zhan FX, Wang YY, Xiao GF, Shi ZL, A pneumonia outbreak associated with a new coronavirus of probable bat origin. *Nature* **579**: 270-273 (2020).

11. Li Q, Wu J, Nie J, Zhang L, Hao H, Liu S, Zhao C, Zhang Q, Liu H, Nie L, Qin H, Wang M, Lu Q, Li X, Sun Q, Liu J, Zhang L, Li X, Huang W, Wang Y, The Impact of Mutations in SARS-CoV-2 Spike on Viral Infectivity and Antigenicity. *Cell* **182**: 1284-1294.e1289 (2020).

12. Wu L, Chen Q, Liu K, Wang J, Han P, Zhang Y, Hu Y, Meng Y, Pan X, Qiao C, Tian S, Du P, Song H, Shi W, Qi J, Wang HW, Yan J, Gao GF, Wang Q, Broad host range of SARS-CoV-2 and the molecular basis for SARS-CoV-2 binding to cat ACE2. *Cell Discov.* **6**: 68 (2020).

13. Chen DY, Chin CV, Kenney D, Tavares AH, Khan N, Conway HL, Liu G, Choudhary MC, Gertje HP, O'Connell AK, Adams S, Kotton DN, Herrmann A, Ensser A, Connor JH, Bosmann M, Li JZ, Gack MU, Baker SC, Kirchdoerfer RN, Kataria Y, Crossland NA, Douam F, Saeed M, Spike and nsp6 are key determinants of SARS-CoV-2 Omicron BA.1 attenuation. *Nature* **615**: 143-150

(2023).

14. Dadonaite B, Crawford KHD, Radford CE, Farrell AG, Yu TC, Hannon WW, Zhou P, Andrabi R, Burton DR, Liu L, Ho DD, Chu HY, Neher RA, Bloom JD, A pseudovirus system enables deep mutational scanning of the full SARS-CoV-2 spike. *Cell* **186**: 1263-1278.e1220 (2023).
15. Gaziano L, Giambartolomei C, Pereira AC, Gaulton A, Posner DC, Swanson SA, Ho YL, Iyengar SK, Kosik NM, Vujkovic M, Gagnon DR, Bento AP, Barrio-Hernandez I, Rönnblom L, Hagberg N, Lundtoft C, Langenberg C, Pietzner M, Valentine D, Gustincich S, Tartaglia GG, Allara E, Surendran P, Burgess S, Zhao JH, Peters JE, Prins BP, Angelantonio ED, Devineni P, Shi Y, Lynch KE, DuVall SL, Garcon H, Thomann LO, Zhou JJ, Gorman BR, Huffman JE, O'Donnell CJ, Tsao PS, Beckham JC, Pyarajan S, Muralidhar S, Huang GD, Ramoni R, Beltrao P, Danesh J, Hung AM, Chang KM, Sun YV, Joseph J, Leach AR, Edwards TL, Cho K, Gaziano JM, Butterworth AS, Casas JP, Actionable druggable genome-wide Mendelian randomization identifies repurposing opportunities for COVID-19. *Nat. Med.* **27**: 668-676 (2021).
16. Brevini T, Maes M, Webb GJ, John BV, Fuchs CD, Buescher G, Wang L, Griffiths C, Brown ML, Scott WE, 3rd, Pereyra-Gerber P, Gelson WTH, Brown S, Dillon S, Muraro D, Sharp J, Neary M, Box H, Tatham L, Stewart J, Curley P, Pertinez H, Forrest S, Mlcochova P, Varankar SS, Darvish-Damavandi M, Mulcahy VL, Kuc RE, Williams TL, Heslop JA, Rossetti D, Tysoe OC, Galanakis V, Vila-Gonzalez M, Crozier TWM, Bargehr J, Sinha S, Upponi SS, Fear C, Swift L, Saeb-Parsy K, Davies SE, Wester A, Hagström H, Melum E, Clements D, Humphreys P, Herriott J, Kijak E, Cox H, Bramwell C, Valentijn A, Illingworth CJR, Dahman B, Bastaich DR, Ferreira RD, Marjot T, Barnes E, Moon AM, Barritt ASt, Gupta RK, Baker S, Davenport AP, Corbett G, Gorgoulis VG, Buczacki SJA, Lee JH, Matheson NJ, Trauner M, Fisher AJ, Gibbs P, Butler AJ, Watson CJE, Mells GF, Dougan G, Owen A, Lohse AW, Vallier L, Sampaziotis F, FXR inhibition may protect from SARS-CoV-2 infection by reducing ACE2.

Nature **615**: 134-142 (2023).

17. Afrache H, Gouret P, Ainouche S, Pontarotti P, Olive D, The butyrophilin (BTN) gene family: from milk fat to the regulation of the immune response. *Immunogenetics* **64**: 781-794 (2012).
18. Tazi-Ahnini R, Henry J, Offer C, Bouissou-Bouchouata C, Mather IH, Pontarotti P, Cloning, localization, and structure of new members of the butyrophilin gene family in the juxta-telomeric region of the major histocompatibility complex. *Immunogenetics* **47**: 55-63 (1997).
19. Wu Y, Bi R, Zeng C, Ma C, Sun C, Li J, Xiao X, Li M, Zhang DF, Zheng P, Sheng N, Luo XJ, Yao YG, Identification of the primate-specific gene BTN3A2 as an additional schizophrenia risk gene in the MHC loci. *EBioMedicine* **44**: 530-541 (2019).
20. Arnett HA, Viney JL, Immune modulation by butyrophilins. *Nat. Rev. Immunol.* **14**: 559-569 (2014).
21. de Groot N, Groen R, Orie V, Bruijnesteijn J, de Groot NG, Doxiadis GGM, Bontrop RE, Analysis of macaque BTN3A genes and transcripts in the extended MHC: conserved orthologs of human γδ T cell modulators. *Immunogenetics* **71**: 545-559 (2019).
22. Yang H, Liu D, Zhao C, Feng B, Lu W, Yang X, Xu M, Zhou W, Jing H, Yang J, Mendelian randomization integrating GWAS and eQTL data revealed genes pleiotropically associated with major depressive disorder. *Transl. Psychiatry* **11**: 225 (2021).
23. Li J, Yoshikawa A, Alliey-Rodriguez N, Meltzer HY, Schizophrenia risk loci from xMHC region were associated with antipsychotic response in chronic schizophrenic patients with persistent positive symptom. *Transl. Psychiatry* **12**: 92 (2022).
24. Kuroda M, Halfmann PJ, Hill-Batorski L, Ozawa M, Lopes TJS, Neumann G, Schoggins JW, Rice CM, Kawaoka Y, Identification of interferon-stimulated genes that attenuate Ebola virus infection. *Nat. Commun.* **11**: 2953 (2020).

25. Pinto RM, Bakshi S, Lytras S, Zakaria MK, Swingler S, Worrell JC, Herder V, Hargrave KE, Varjak M, Cameron-Ruiz N, Collados Rodriguez M, Varela M, Wickenhagen A, Loney C, Pei Y, Hughes J, Valette E, Turnbull ML, Furnon W, Gu Q, Orr L, Taggart A, Diebold O, Davis C, Boutell C, Grey F, Hutchinson E, Digard P, Monne I, Wootton SK, MacLeod MKL, Wilson SJ, Palmarini M, BTN3A3 evasion promotes the zoonotic potential of influenza A viruses. *Nature* **619**: 338-347 (2023).

26. Li M, Ferretti M, Ying B, Descamps H, Lee E, Dittmar M, Lee JS, Whig K, Kamalia B, Dohnalová L, Uhr G, Zarkoob H, Chen YC, Ramage H, Ferrer M, Lynch K, Schultz DC, Thaiss CA, Diamond MS, Cherry S, Pharmacological activation of STING blocks SARS-CoV-2 infection. *Sci. Immunol.* **6**: eabi9007 (2021).

27. Overmyer KA, Shishkova E, Miller IJ, Balnis J, Bernstein MN, Peters-Clarke TM, Meyer JG, Quan Q, Muehlbauer LK, Trujillo EA, He Y, Chopra A, Chieng HC, Tiwari A, Judson MA, Paulson B, Brademan DR, Zhu Y, Serrano LR, Linke V, Drake LA, Adam AP, Schwartz BS, Singer HA, Swanson S, Mosher DF, Stewart R, Coon JJ, Jaitovich A, Large-Scale Multi-omic Analysis of COVID-19 Severity. *Cell Syst.* **12**: 23-40.e27 (2021).

28. Dean MJ, Ochoa JB, Sanchez-Pino MD, Zabaleta J, Garai J, Del Valle L, Wyczechowska D, Baiamonte LB, Philbrook P, Majumder R, Vander Heide RS, Dunkenberger L, Thylur RP, Nossaman B, Roberts WM, Chapple AG, Wu J, Hicks C, Collins J, Luke B, Johnson R, Koul HK, Rees CA, Morris CR, Garcia-Diaz J, Ochoa AC, Severe COVID-19 Is characterized by an impaired type I interferon response and elevated levels of arginase producing granulocytic myeloid derived suppressor cells. *Front Immunol.* **12**: 695972 (2021).

29. Bost P, De Sanctis F, Canè S, Ugel S, Donadello K, Castellucci M, Eyal D, Fiore A, Anselmi C, Barouni RM, Trovato R, Caligola S, Lamolinara A, Iezzi M, Facciotti F, Mazzariol A, Gibellini D, De Nardo P, Tacconelli E, Gottin L, Polati E, Schwikowski B, Amit I, Bronte V, Deciphering the state of immune silence in fatal COVID-19 patients. *Nat. Commun.* **12**: 1428 (2021).

30. Yamashiro H, Yoshizaki S, Tadaki T, Egawa K, Seo N, Stimulation of human butyrophilin 3 molecules results in negative regulation of cellular immunity. *J. Leukoc. Biol.* **88**: 757-767 (2010).

31. Consortium G, The Genotype-Tissue Expression (GTEx) project. *Nat. Genet.* **45**: 580-585 (2013).

32. Melms JC, Biermann J, Huang H, Wang Y, Nair A, Tagore S, Katsyv I, Rendeiro AF, Amin AD, Schapiro D, Frangieh CJ, Luoma AM, Filliol A, Fang Y, Ravichandran H, Clausi MG, Alba GA, Rogava M, Chen SW, Ho P, Montoro DT, Kornberg AE, Han AS, Bakhoum MF, Anandasabapathy N, Suárez-Fariñas M, Bakhoum SF, Bram Y, Borczuk A, Guo XV, Lefkowitch JH, Marboe C, Lagana SM, Del Portillo A, Tsai EJ, Zorn E, Markowitz GS, Schwabe RF, Schwartz RE, Elemento O, Saqi A, Hibshoosh H, Que J, Izar B, A molecular single-cell lung atlas of lethal COVID-19. *Nature* **595**: 114-119 (2021).

33. Delorey TM, Ziegler CGK, Heimberg G, Normand R, Yang Y, Segerstolpe Å, Abbondanza D, Fleming SJ, Subramanian A, Montoro DT, Jagadeesh KA, Dey KK, Sen P, Slyper M, Pita-Juárez YH, Phillips D, Biermann J, Bloom-Ackermann Z, Barkas N, Ganna A, Gomez J, Melms JC, Katsyv I, Normandin E, Naderi P, Popov YV, Raju SS, Niezen S, Tsai LT, Siddle KJ, Sud M, Tran VM, Vellarikkal SK, Wang Y, Amir-Zilberstein L, Atri DS, Beechem J, Brook OR, Chen J, Divakar P, Dorceus P, Engreitz JM, Essene A, Fitzgerald DM, Fropf R, Gazal S, Gould J, Grzyb J, Harvey T, Hecht J, Hether T, Jané-Valbuena J, Leney-Greene M, Ma H, McCabe C, McLoughlin DE, Miller EM, Muus C, Niemi M, Padera R, Pan L, Pant D, Pe'er C, Pfiffner-Borges J, Pinto CJ, Plaisted J, Reeves J, Ross M, Rudy M, Rueckert EH, Siciliano M, Sturm A, Todres E, Waghray A, Warren S, Zhang S, Zollinger DR, Cosimi L, Gupta RM, Hacohen N, Hibshoosh H, Hide W, Price AL, Rajagopal J, Tata PR, Riedel S, Szabo G, Tickle TL, Ellinor PT, Hung D, Sabeti PC, Novak R, Rogers R, Ingber DE, Jiang ZG, Juric D, Babadi M, Farhi SL, Izar B, Stone JR, Vlachos IS, Solomon IH, Ashenberg O, Porter CBM, Li B, Shalek AK, Villani AC, Rozenblatt-Rosen O,

Regev A, COVID-19 tissue atlases reveal SARS-CoV-2 pathology and cellular targets. *Nature* **595**: 107-113 (2021).

34. Ma Q, Ma W, Song TZ, Wu Z, Liu Z, Hu Z, Han JB, Xu L, Zeng B, Wang B, Sun Y, Yu DD, Wu Q, Yao YG, Zheng YT, Wang X, Single-nucleus transcriptomic profiling of multiple organs in a rhesus macaque model of SARS-CoV-2 infection. *Zool. Res.* **43**: 1041-1062 (2022).
35. Gao CC, Li M, Deng W, Ma CH, Chen YS, Sun YQ, Du T, Liu QL, Li WJ, Zhang B, Sun L, Liu SM, Li F, Qi F, Qu Y, Ge X, Liu J, Wang P, Niu Y, Liang Z, Zhao YL, Huang B, Peng XZ, Yang Y, Qin C, Tong WM, Yang YG, Differential transcriptomic landscapes of multiple organs from SARS-CoV-2 early infected rhesus macaques. *Protein Cell* **13**: 920-939 (2022).
36. Harcourt J, Tamin A, Lu X, Kamili S, Sakthivel SK, Murray J, Queen K, Tao Y, Paden CR, Zhang J, Li Y, Uehara A, Wang H, Goldsmith C, Bullock HA, Wang L, Whitaker B, Lynch B, Gautam R, Schindewolf C, Lokugamage KG, Scharton D, Plante JA, Mirchandani D, Widen SG, Narayanan K, Makino S, Ksiazek TG, Plante KS, Weaver SC, Lindstrom S, Tong S, Menachery VD, Thornburg NJ, Severe acute respiratory syndrome coronavirus 2 from patient with coronavirus disease, United States. *Emerg. Infect. Dis.* **26**: 1266-1273 (2020).
37. Pang W, Lu Y, Zhao YB, Shen F, Fan CF, Wang Q, He WQ, He XY, Li ZK, Chen TT, Yang CX, Li YZ, Xiao SX, Zhao ZJ, Huang XS, Luo RH, Yang LM, Zhang M, Dong XQ, Li MH, Feng XL, Zhou QC, Qu W, Jiang S, Ouyang S, Zheng YT, A variant-proof SARS-CoV-2 vaccine targeting HR1 domain in S2 subunit of spike protein. *Cell Res.* **32**: 1068-1085 (2022).
38. Xu L, Yu D, Yao YL, Gu T, Zheng X, Wu Y, Luo RH, Zheng YT, Zhong J, Yao YG, Tupaia MAVS is a dual target during Hepatitis C virus infection for innate immune evasion and viral replication via NF-κB. *J. Immunol.* **205**: 2091-2099 (2020).
39. Shang J, Wan Y, Luo C, Ye G, Geng Q, Auerbach A, Li F, Cell entry mechanisms of SARS-CoV-2. *Proc. Natl. Acad. Sci. U. S. A.* **117**: 11727-11734 (2020).

40. Liu L, Wang P, Nair MS, Yu J, Rapp M, Wang Q, Luo Y, Chan JFW, Sahi V, Fig.ueroa A, Guo XV, Cerutti G, Bimela J, Gorman J, Zhou T, Chen Z, Yuen K-Y, Kwong PD, Sodroski JG, Yin MT, Sheng Z, Huang Y, Shapiro L, Ho DD, Potent neutralizing antibodies against multiple epitopes on SARS-CoV-2 spike. *Nature* **584**: 450-456 (2020).

41. Piccoli L, Park YJ, Tortorici MA, Czudnochowski N, Walls AC, Beltramello M, Silacci-Fregni C, Pinto D, Rosen LE, Bowen JE, Acton OJ, Jaconi S, Guarino B, Minola A, Zatta F, Sprugasci N, Bassi J, Peter A, De Marco A, Nix JC, Mele F, Jovic S, Rodriguez BF, Gupta SV, Jin F, Piumatti G, Lo Presti G, Pellanda AF, Biggiogero M, Tarkowski M, Pizzuto MS, Cameroni E, Havenar-Daughton C, Smithey M, Hong D, Lepori V, Albanese E, Ceschi A, Bernasconi E, Elzi L, Ferrari P, Garzoni C, Riva A, Snell G, Sallusto F, Fink K, Virgin HW, Lanzavecchia A, Corti D, Veesler D, Mapping neutralizing and immunodominant sites on the SARS-CoV-2 spike receptor-binding domain by structure-guided high-resolution serology. *Cell* **183**: 1024-1042.e1021 (2020).

42. Shi R, Zeng J, Xu L, Wang F, Duan X, Wang Y, Wu Z, Yu D, Huang Q, Yao YG, Yan J, A combination vaccine against SARS-CoV-2 and H1N1 influenza based on receptor binding domain trimerized by six-helix bundle fusion core. *EBioMedicine* **85**: 104297 (2022).

43. Lan J, Ge J, Yu J, Shan S, Zhou H, Fan S, Zhang Q, Shi X, Wang Q, Zhang L, Wang X, Structure of the SARS-CoV-2 spike receptor-binding domain bound to the ACE2 receptor. *Nature* **581**: 215-220 (2020).

44. Sun X, Liu Y, Huang Z, Xu W, Hu W, Yi L, Liu Z, Chan H, Zeng J, Liu X, Chen H, Yu J, Chan FKL, Ng SC, Wong SH, Wang MH, Gin T, Joynt GM, Hui DSC, Zou X, Shu Y, Cheng CHK, Fang S, Luo H, Lu J, Chan MTV, Zhang L, Wu WKK, SARS-CoV-2 non-structural protein 6 triggers NLRP3-dependent pyroptosis by targeting ATP6AP1. *Cell Death Differ.* **29**: 1240-1254 (2022).

45. Dagotto G, Mercado NB, Martinez DR, Hou YJ, Nkolola JP, Carnahan RH, Crowe JE, Jr., Baric RS, Barouch DH, Comparison of subgenomic and total RNA in

SARS-CoV-2 challenged rhesus macaques. *J. Virol.* **95**: e02370-20 (2021).

46. Pfaender S, Mar KB, Michailidis E, Kratzel A, Boys IN, V'Kovski P, Fan W, Kelly JN, Hirt D, Ebert N, Stalder H, Kleine-Weber H, Hoffmann M, Hoffmann HH, Saeed M, Dijkman R, Steinmann E, Wight-Carter M, McDougal MB, Hanners NW, Pöhlmann S, Gallagher T, Todt D, Zimmer G, Rice CM, Schoggins JW, Thiel V, LY6E impairs coronavirus fusion and confers immune control of viral disease. *Nat. Microbiol.* **5**: 1330-1339 (2020).
47. Xu D, Jiang W, Wu L, Gaudet RG, Park ES, Su M, Cheppali SK, Cheemarla NR, Kumar P, Uchil PD, Grover JR, Foxman EF, Brown CM, Stansfeld PJ, Bewersdorf J, Mothes W, Karatekin E, Wilen CB, MacMicking JD, PLSCR1 is a cell-autonomous defence factor against SARS-CoV-2 infection. *Nature* **619**: 819-827 (2023).
48. Samelson AJ, Tran QD, Robinot R, Carrau L, Rezelj VV, Kain AM, Chen M, Ramadoss GN, Guo X, Lim SA, Lui I, Nuñez JK, Rockwood SJ, Wang J, Liu N, Carlson-Stevermer J, Oki J, Maures T, Holden K, Weissman JS, Wells JA, Conklin BR, TenOever BR, Chakrabarti LA, Vignuzzi M, Tian R, Kampmann M, BRD2 inhibition blocks SARS-CoV-2 infection by reducing transcription of the host cell receptor ACE2. *Nat. Cell Biol.* **24**: 24-34 (2022).
49. Hadjadj J, Yatim N, Barnabei L, Corneau A, Boussier J, Smith N, Péré H, Charbit B, Bondet V, Chenevier-Gobeaux C, Breillat P, Carlier N, Gauzit R, Morbieu C, Pène F, Marin N, Roche N, Szwebel TA, Merkling SH, Treluyer JM, Veyer D, Mouthon L, Blanc C, Tharaux PL, Rozenberg F, Fischer A, Duffy D, Rieux-Laucat F, Kernéis S, Terrier B, Impaired type I interferon activity and inflammatory responses in severe COVID-19 patients. *Science* **369**: 718-724 (2020).
50. Damas J, Hughes GM, Keough KC, Painter CA, Persky NS, Corbo M, Hiller M, Koepfli KP, Pfenning AR, Zhao H, Genereux DP, Swofford R, Pollard KS, Ryder OA, Nweeia MT, Lindblad-Toh K, Teeling EC, Karlsson EK, Lewin HA, Broad host range of SARS-CoV-2 predicted by comparative and structural

analysis of ACE2 in vertebrates. *Proc. Natl. Acad. Sci. U. S. A.* **117**: 22311-22322 (2020).

51. Vantourout P, Laing A, Woodward MJ, Zlatareva I, Apolonia L, Jones AW, Snijders AP, Malim MH, Hayday AC, Heteromeric interactions regulate butyrophilin (BTN) and BTN-like molecules governing γδ T cell biology. *Proc. Natl. Acad. Sci. U. S. A.* **115**: 1039-1044 (2018).
52. Zheng Y, Li S, Song K, Ye J, Li W, Zhong Y, Feng Z, Liang S, Cai Z, Xu K, A broad antiviral strategy: inhibitors of human DHODH pave the way for host-targeting antivirals against emerging and re-emerging viruses. *Viruses* **14**: 928 (2022).
53. Mahajan S, Choudhary S, Kumar P, Tomar S, Antiviral strategies targeting host factors and mechanisms obliging +ssRNA viral pathogens. *Bioorg. Med. Chem.* **46**: 116356 (2021).
54. Nasserie T, Hittle M, Goodman SN, Assessment of the frequency and variety of persistent symptoms among patients With COVID-19: A systematic review. *JAMA Netw. Open* **4**: e2111417 (2021).
55. Monje M, Iwasaki A, The neurobiology of long COVID. *Neuron* **110**: 3484-3496 (2022).
56. Ma G, Zhang DF, Zou QC, Xie X, Xu L, Feng XL, Li X, Han JB, Yu D, Deng ZH, Qu W, Long J, Li MH, Yao YG, Zeng J, SARS-CoV-2 Spike protein S2 subunit modulates γ-secretase and enhances amyloid-β production in COVID-19 neuropathy. *Cell Discov.* **8**: 99 (2022).
57. Fernández-Castañeda A, Lu P, Geraghty AC, Song E, Lee MH, Wood J, O'Dea MR, Dutton S, Shamardani K, Nwangwu K, Mancusi R, Yalçın B, Taylor KR, Acosta-Alvarez L, Malacon K, Keough MB, Ni L, Woo PJ, Contreras-Esquivel D, Toland AMS, Gehlhausen JR, Klein J, Takahashi T, Silva J, Israelow B, Lucas C, Mao T, Peña-Hernández MA, Tabachnikova A, Homer RJ, Tabacof L, Tosto-Mancuso J, Breyman E, Kontorovich A, McCarthy D, Quezado M, Vogel H, Hefti MM, Perl DP, Liddelow S, Folkerth R, Putrino D, Nath A, Iwasaki A, Monje M, Mild respiratory COVID can cause multi-lineage neural cell and

myelin dysregulation. *Cell* **185**: 2452-2468.e2416 (2022).

58. Ribeiro M, Brigas HC, Temido-Ferreira M, Pousinha PA, Regen T, Santa C, Coelho JE, Marques-Morgado I, Valente CA, Omenetti S, Stockinger B, Waisman A, Manadas B, Lopes LV, Silva-Santos B, Ribot JC, Meningeal γδ T cell-derived IL-17 controls synaptic plasticity and short-term memory. *Sci. Immunol.* **4**: eaay5199 (2019).
59. Gu S, Borowska MT, Boughter CT, Adams EJ, Butyrophilin3A proteins and Vγ9Vδ2 T cell activation. *Semin. Cell Dev. Biol.* **84**: 65-74 (2018).
60. Feng XL, Yu D, Zhang M, Li X, Zou QC, Ma W, Han JB, Xu L, Yang C, Qu W, Deng ZH, Long J, Long Y, Li M, Yao YG, Dong XQ, Zeng J, Li MH, Characteristics of replication and pathogenicity of SARS-CoV-2 Alpha and Delta isolates. *Virol. Sin.* **37**: 804-812 (2022).
61. Yu D, Long Y, Xu L, Han JB, Xi J, Xu J, Yang LX, Feng XL, Zou QC, Qu W, Lin J, Li MH, Yao YG, Infectivity of SARS-CoV-2 and protection against reinfection in rats. *Zool. Res.* **43**: 945-948 (2022).
62. Xu L, Yu DD, Ma YH, Yao YL, Luo RH, Feng XL, Cai HR, Han JB, Wang XH, Li MH, Ke CW, Zheng YT, Yao YG, COVID-19-like symptoms observed in Chinese tree shrews infected with SARS-CoV-2. *Zool. Res.* **41**: 517-526 (2020).
63. Xu L, Yu D, Fan Y, Peng L, Wu Y, Yao YG, Loss of RIG-I leads to a functional replacement with MDA5 in the Chinese tree shrew. *Proc. Natl. Acad. Sci. U. S. A.* **113**: 10950-10955 (2016).
64. Bolger AM, Lohse M, Usadel B, Trimmomatic: a flexible trimmer for Illumina sequence data. *Bioinformatics* **30**: 2114-2120 (2014).
65. Dobin A, Davis CA, Schlesinger F, Drenkow J, Zaleski C, Jha S, Batut P, Chaisson M, Gingeras TR, STAR: ultrafast universal RNA-seq aligner. *Bioinformatics* **29**: 15-21 (2013).
66. Li B, Dewey CN, RSEM: accurate transcript quantification from RNA-Seq data with or without a reference genome. *BMC Bioinformatics* **12**: 323 (2011).
67. Tian Y, Carpp LN, Miller HER, Zager M, Newell EW, Gottardo R, Single-cell

immunology of SARS-CoV-2 infection. *Nat. Biotechnol.* **40**: 30-41 (2022).

68. Eraslan G, Drokhlyansky E, Anand S, Fiskin E, Subramanian A, Slyper M, Wang J, Van Wittenberghe N, Rouhana JM, Waldman J, Ashenberg O, Lek M, Dionne D, Win TS, Cuoco MS, Kuksenko O, Tsankov AM, Branton PA, Marshall JL, Greka A, Getz G, Segrè AV, Aguet F, Rozenblatt-Rosen O, Ardlie KG, Regev A, Single-nucleus cross-tissue molecular reference maps toward understanding disease gene function. *Science* **376**: eabl4290 (2022).
69. Blanco-Melo D, Nilsson-Payant BE, Liu WC, Uhl S, Hoagland D, Møller R, Jordan TX, Oishi K, Panis M, Sachs D, Wang TT, Schwartz RE, Lim JK, Albrecht RA, tenOever BR, Imbalanced host response to SARS-CoV-2 drives development of COVID-19. *Cell* **181**: 1036-1045.e1039 (2020).
70. Daamen AR, Bachali P, Owen KA, Kingsmore KM, Hubbard EL, Labonte AC, Robl R, Shrotri S, Grammer AC, Lipsky PE, Comprehensive transcriptomic analysis of COVID-19 blood, lung, and airway. *Sci. Rep.* **11**: 7052 (2021).
71. Love MI, Huber W, Anders S, Moderated estimation of fold change and dispersion for RNA-seq data with DESeq2. *Genome Biol.* **15**: 550 (2014).
72. Ritchie ME, Phipson B, Wu D, Hu Y, Law CW, Shi W, Smyth GK, limma powers differential expression analyses for RNA-sequencing and microarray studies. *Nucleic Acids Res.* **43**: e47 (2015).
73. Sun S, Cai Y, Song TZ, Pu Y, Cheng L, Xu H, Sun J, Meng C, Lin Y, Huang H, Zhao F, Zhang S, Gao Y, Han JB, Feng XL, Yu DD, Zhu Y, Gao P, Tang H, Zhao J, Zhang Z, Yang J, Hu Z, Fu YX, Zheng YT, Peng H, Interferon-armed RBD dimer enhances the immunogenicity of RBD for sterilizing immunity against SARS-CoV-2. *Cell Res.* **31**: 1011-1023 (2021).
74. Liu Y, Dai L, Feng X, Gao R, Zhang N, Wang B, Han J, Zou Q, Guo X, Zhu H, Liu J, Qin C, Zhang Y, Bao L, Li M, Fast and long-lasting immune response to S-trimer COVID-19 vaccine adjuvanted by PIKA. *Mol. Biomed.* **2**: 29 (2021).
75. Zeng J, Xie X, Feng XL, Xu L, Han JB, Yu D, Zou QC, Liu Q, Li X, Ma G, Li MH, Yao YG, Specific inhibition of the NLRP3 inflammasome suppresses immune

overactivation and alleviates COVID-19 like pathology in mice. *EBioMedicine* **75**: 103803 (2022).

Figure legends

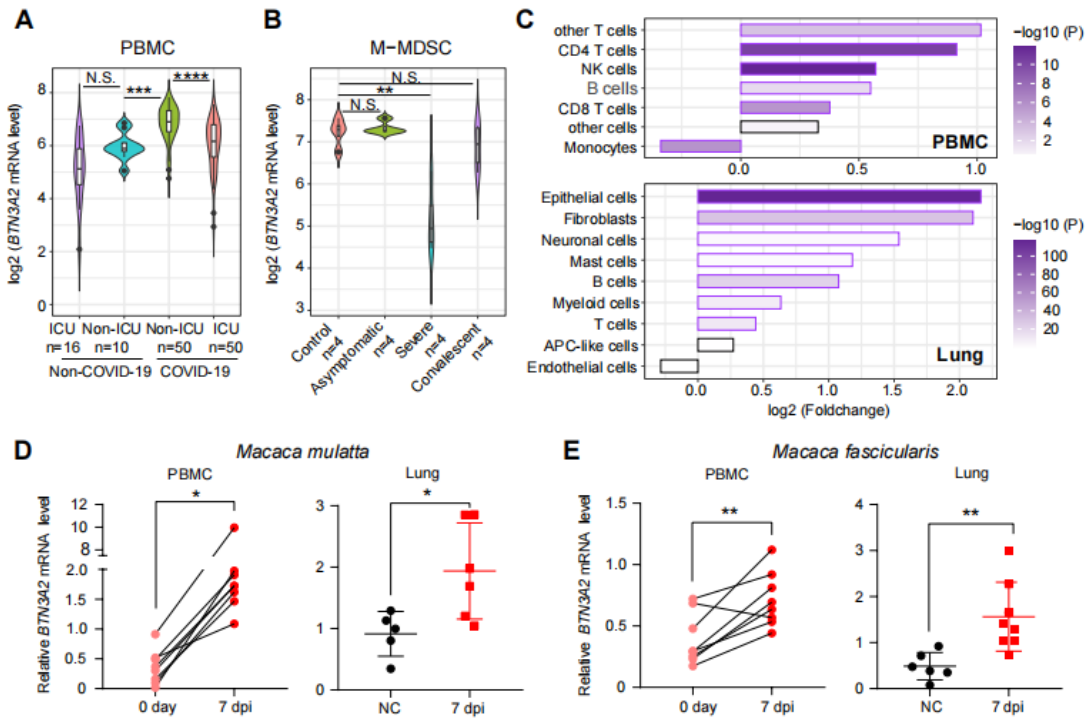

Fig. 1. BTN3A2 was up-regulated in COVID-19 patients and NHPs infected with SARS-CoV-2

A: Violin plot of *BTN3A2* mRNA levels in PBMCs from COVID-19 patients with (ICU COVID-19) or without ICU experience (Non-ICU COVID-19) compared to healthy individuals (Non-ICU Non-COVID-19) and individuals in ICU but not for COVID-19 (ICU Non-COVID-19). Original dataset (GSE157103) was reported in Overmyer et al. (27).

B: Violin plot of *BTN3A2* mRNA levels in M-MDSCs based on the GSE178824 dataset (28). *BTN3A2* mRNA expression was normalized by trimmed mean of M-values.

A-B: *BTN3A2* mRNA levels were normalized by transcripts per million (TPM). Gene expression level was determined as log2 fold-change. Purple borders indicate $P<0.05$ and black borders indicate $P>0.05$. Statistical significance was assessed by two-sided *t*-test.

C: Histogram showing up-regulation of *BTN3A2* mRNA levels in PBMCs (*upper*) and lung tissues (*lower*) of COVID-19 patients based on datasets reported in Tian et al. (67) and Melms et al. (32). Statistical significance was assessed by two-sided Wilcox rank sum test.

D-E: *BTN3A2* mRNA levels were up-regulated in PBMCs (*left*) and lung tissues (*right*) of rhesus (D) and cynomolgus monkeys (E) challenged with or without SARS-CoV-2. For PBMCs, samples were collected before SARS-CoV-2 infection (0 day) and 7 dpi. For lung tissues, samples were collected from animals without SARS-CoV-2 infection (NC) and animals infected with SARS-CoV-2 at 7 dpi. *BTN3A2* mRNA level was measured by qRT-PCR and normalized to *GAPDH*. *, $P < 0.05$; **, $P < 0.01$; paired *t*-test.

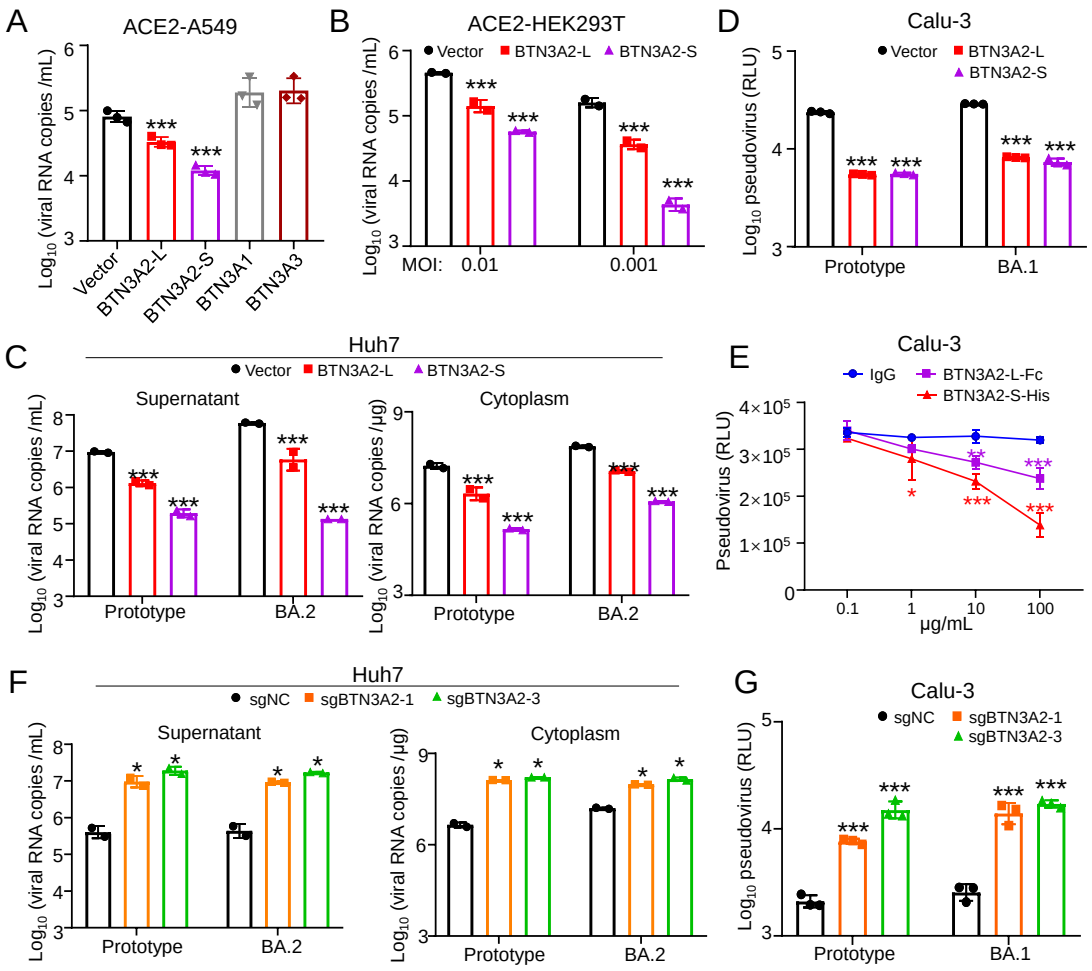

Fig. 2. BTN3A2 was identified as a potent restriction factor of SARS-CoV-2 infection

A: Overexpression of BTN3A family members inhibited SARS-CoV-2 replication in A549 cells overexpressing human ACE2 (ACE2-A549). ACE2-A549 cells (1×10^5) were transfected with indicated expression vector (BTN3A2-L, BTN3A2-S, BTN3A1, or BTN3A3) or empty vector (Vector) (each 1 μg) for 24 h, then infected with SARS-CoV-2 (MOI=0.01) for 24 h. Cells were harvested and quantified to determine SARS-CoV-2 copies by qRT-PCR.

B: Overexpression of BTN3A2 inhibited SARS-CoV-2 replication in HEK293T cells

overexpressing human ACE2 (ACE2-HEK293T). ACE2-HEK293T cells (5×10^4) were transfected with indicated expression vector or empty vector (each 1 μg) for 24 h, then infected with SARS-CoV-2 (MOI=0.01 or 0.001) for 24 h and harvested for quantification of SARS-CoV-2 copies.

C: Stable expression of BTN3A2 in Huh7 cells inhibited SARS-CoV-2 replication. Huh7 cells were transfected with lentiviruses carrying empty vector (Vector), BTN3A2-L, and BTN3A2-S to establish stable cell lines. Each cell line (1×10^5 cells) was treated with DOX (1 μg/mL) for 24 h, then challenged with the SARS-CoV-2 prototype or BA.2 (MOI=1) for 24 h. The culture medium (supernatant, *left*) and cell lysates (cytoplasm, *right*) were collected to quantify SARS-CoV-2 copies.

D: Stable expression of BTN3A2 in Huh7 cells inhibited replication of VSV pseudotyped SARS-CoV-2 (prototype and BA.1). The procedure was similar to that in (C). Cells were collected, and viral infectivity was quantified based on *Renilla* luciferase activity using a *Renilla* Luciferase Assay Kit (Promega, Madison, WI, USA).

E: Incubation with BTN3A2 isoforms (BTN3A2-L-Fc and BTN3A2-S-His) inhibited replication of VSV pseudotyped SARS-CoV-2 (BA.1) in Calu-3 cells. IgG treatment was used as a negative control. Cells were incubated with BTN3A2 isoform or IgG for 1 h, then infected with VSV pseudotyped SARS-CoV-2 (BA.1) for 24 h and harvested to determine viral infectivity.

F: Knockout of BTN3A2 increased SARS-CoV-2 replication in Huh7 cells. Cells transfected with indicated sgRNAs (sgNC, negative control; sgBTN3A2-1 and

sgBTN3A2-3, both targeting *BTN3A2*) were infected with SARS-CoV-2 prototype or BA.2 (MOI=1) for 24 h, then harvested to quantify SARS-CoV-2 copies.

G: Knockout of BTN3A2 increased VSV pseudotyped SARS-CoV-2 (prototype and BA.1) replication in Calu-3 cells. The procedure for determining viral infectivity was the same as that in (D).

Data are representative of three independent experiments with similar results and are presented as mean±standard deviation (SD). Significance was determined compared to Vector (A, B, C, and D), IgG control at each dilution (E), or sgNC (F and G). *, $P<0.05$; **, $P<0.01$, ***, $P<0.001$; one-way analysis of variance (ANOVA).

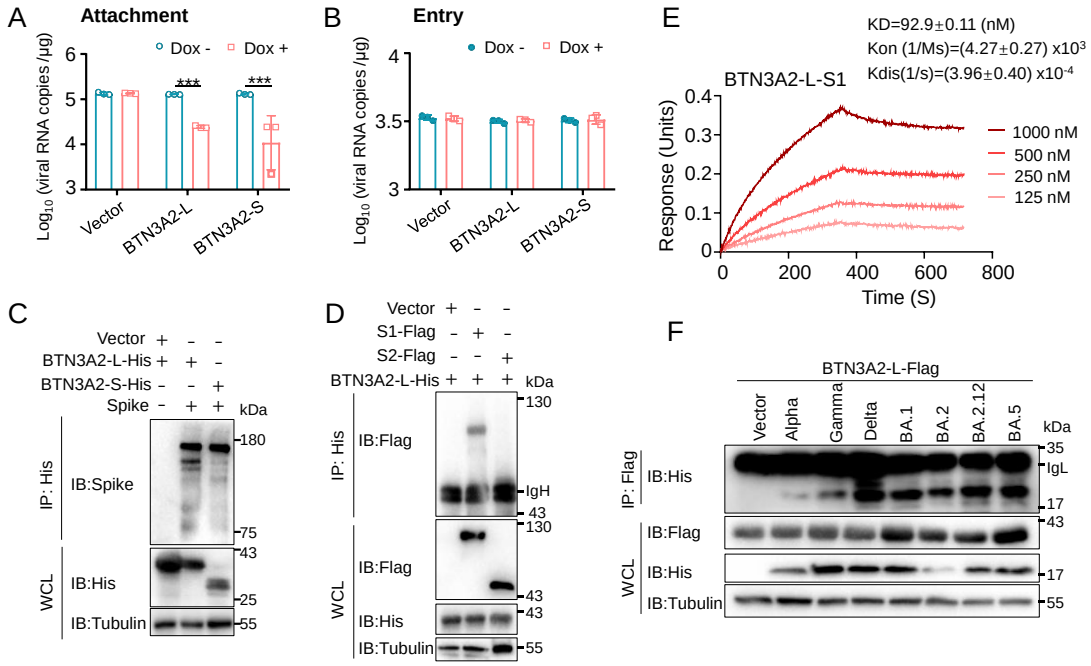

Fig. 3. BTN3A2 inhibited SARS-CoV-2 entry and interacted with Spike protein via its RBD

A: Stable expression of BTN3A2 suppressed SARS-CoV-2 attachment to the cell. Huh7 cells with or without BTN3A2-L and BTN3A2-S expression were treated with DOX (1 μg/mL) for 48 h, then incubated with SARS-CoV-2 (MOI=1) on ice at 4 °C for 1 h. Cells were washed by PBS three times and harvested to measure viral RNA copies based on SARS-CoV-2 *N* gene level.

B: Stable expression of BTN3A2 did not affect cellular entry of SARS-CoV-2. For viral internalization, Huh7 cells were processed using the same procedures as those in (A), with the cells then replenished in a 37 °C incubator for 1 h. Pronase (1 mg/mL) was added to the cells at 37 °C for 10 min before RNA extraction. Viral copies were quantified using the same procedure as that in (A).

C: BTN3A2 interacted with the SARS-CoV-2 Spike protein. HEK293T cells (1×10^7) were co-transfected with expression vector for BTN3A2 (BTN3A2-L-His or BTN3A2-S-His, each 5 μg) and Spike protein (5 μg) for 48 h. Whole-cell lysates were immunoprecipitated (IP) using anti-His antibodies. Immunoblotting (IB) for His (BTN3A2-L-His or BTN3A2-S-His), Spike, and Tubulin was performed using anti-His, anti-Spike, and anti-Tubulin antibodies, respectively.

D: BTN3A2-L interacted with the S1 subunit but not the S2 subunit of the Spike protein. Spike S1 and S2 subunits were Flag-tagged.

E: Biolayer interferometry analysis of Spike S1 protein binding to immobilized BTN3A2-L-His. Different concentrations (1 000, 500, 250, and 125 nM, corresponding to kinetic curves from top to bottom) of Spike S1 protein were used.

F: BTN3A2 interacted with Spike RBDs of different SARS-CoV-2 variants. Procedures for IP and IB in (D) and (F) are the same as those in (C).

Data are representative of three independent experiments with similar results and are presented as mean±SD. Significance was determined using one-way ANOVA. ***, $P<0.001$.

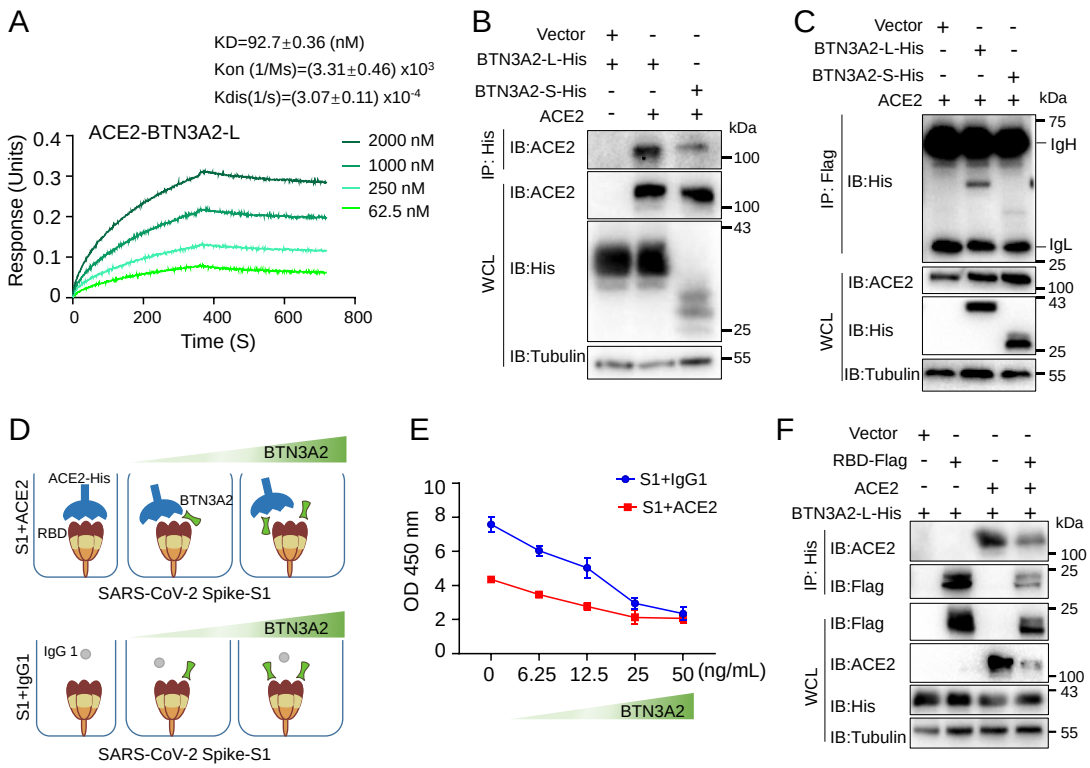

Fig. 4. BTN3A2 competed with ACE2 to bind to the Spike protein

A: Biolayer interferometry analysis of BTN3A2-L binding to immobilized ACE2-Fc. Different concentrations of BTN3A2-L (2 000, 1 000, 250, and 62.5 nM; corresponding to kinetic curves from top to bottom) were used.

B: BTN3A2 isoforms interacted with ACE2.

C: ACE2 interacted with BTN3A2-L.

D-E: Competition ELISA analysis of competitive binding of BTN3A2-L with Spike RBD (Spike-RBD). D: Schematic of competition assays. E: Competition between ACE2 (ACE2-His-tagged) and BTN3A2-L (BTN3A2) for immobilized SARS-CoV-2 spike S1 subunit (S1-Fc). ACE2 and S1-Fc proteins or human IgG1-Fc and S1-Fc protein were incubated for 12 h, followed by the addition of three dilution series of BTN3A2-L-His. Amount of S1 protein remaining in the presence of the competitor

was determined by antihuman HRP through a colorimetric readout.

F: BTN3A2-L competed with ACE2 to bind to the Spike RBD. Procedures for IP and IB in (B-C) and (F) were similar to those in Fig. 3C.

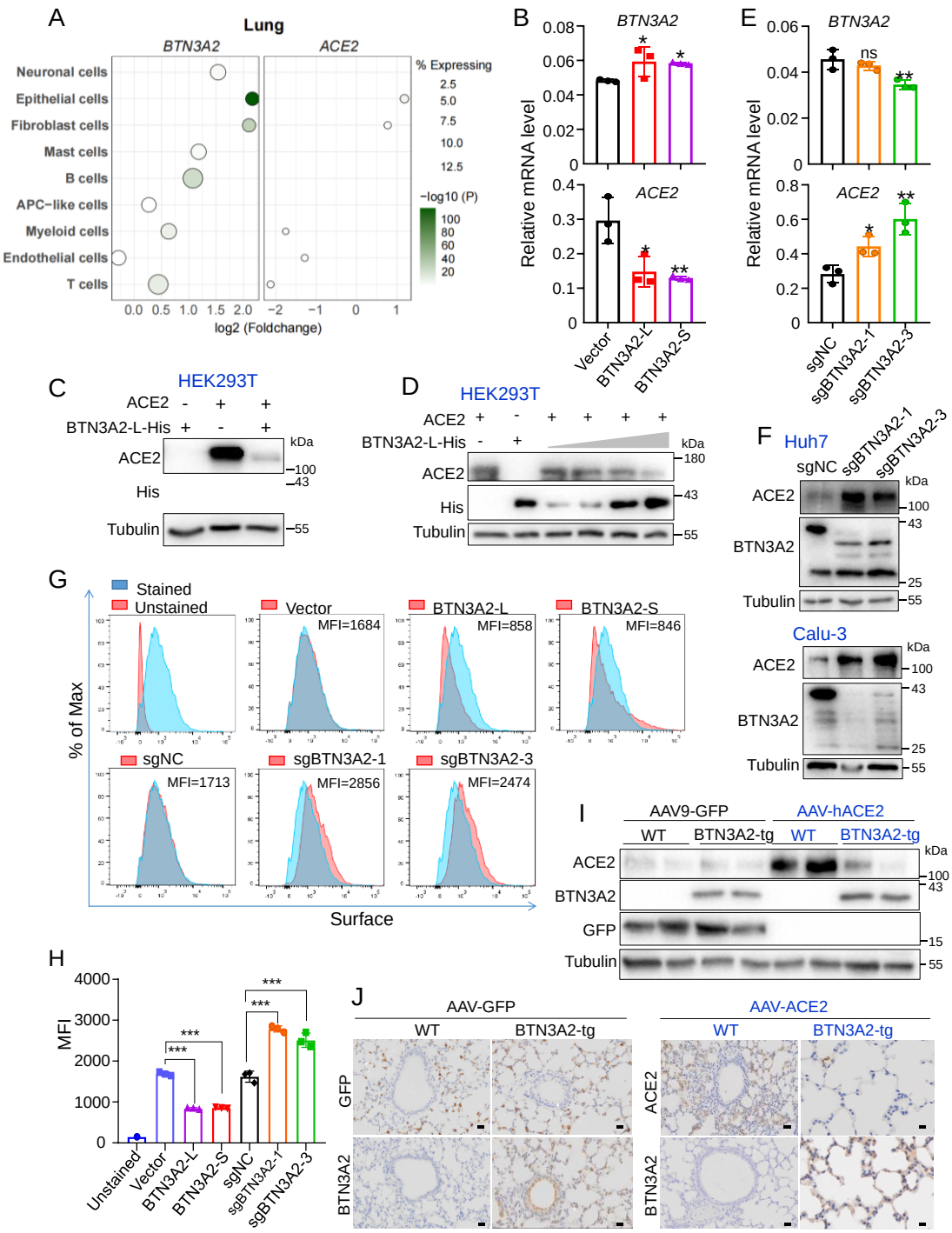

Fig. 5. BTN3A2 inhibited ACE2 expression

A: Differential expression of *BTN3A2* and *ACE2* in scRNA-seq dataset of lung tissues from COVID-19 patients and uninfected individuals. Original dataset was reported in Melms et al. (32). Significance was assessed by two-sided Wilcox rank sum test.

B: Stable expression of BTN3A2 decreased *ACE2* mRNA level in Huh7 cells. RNA was extracted from cells (each group 1×10^5 cells) with stable expression of BTN3A2-L and BTN3A2-S, or empty vector (Vector). *BTN3A2* and *ACE2* mRNA levels were measured by qRT-PCR, with normalization to *GAPDH*.

C: Overexpression of BTN3A2-L suppressed ACE2 protein expression in HEK293T cells. Cells (5×10^5) were transfected with indicated expression vector or empty vector (each 1.25 μg) for 48 h, then harvested for western blotting.

D: Dose-dependent inhibitory effect of BTN3A2-L on ACE2 protein expression. HEK293T cells (5×10^5) were transfected with indicated expression vector or empty vector (each 0.5 μg), together with increased BTN3A2-L-His (250, 500, 750, and 15 000 ng, with empty vector to reach a total amount of 2.5 μg of plasmid) for 48 h, then harvested for western blotting.

E: Knockout of BTN3A2 increased *ACE2* mRNA level in Huh7 cells. The procedure was similar to that in (B).

F: Knockout of BTN3A2 promoted ACE2 protein expression in Huh7 (*upper*) and Calu-3 (*lower*) cells.

G-H: Flow cytometry was conducted to analyze surface ACE2 in Calu-3 cells with BTN3A2 overexpression or knockout. Cell surface expression of ACE2 was measured (G) and calculated as mean fluorescence intensity (MFI, n=3) (H).

I: ACE2 protein levels in BTN3A2-tg and WT mice infected with indicated AAV-GFP and AAV-hACE2. Immunoblotting for hACE2, BTN3A2, GFP, and Tubulin was performed using anti-ACE2, anti-BTN3A2, anti-GFP, and anti-Tubulin antibodies,

respectively.

J: Immunohistochemical staining of ACE2 and BTN3A2 lung tissues in (I). Scale bar, 100 μm.

Data are representative of three independent experiments with similar results and are presented as mean±SD. Significance was determined compared to Vector (B and H) or sgNC (E). ns, not significant; *, P <0.05; **, P<0.01, ***, P<0.001; one-way ANOVA.

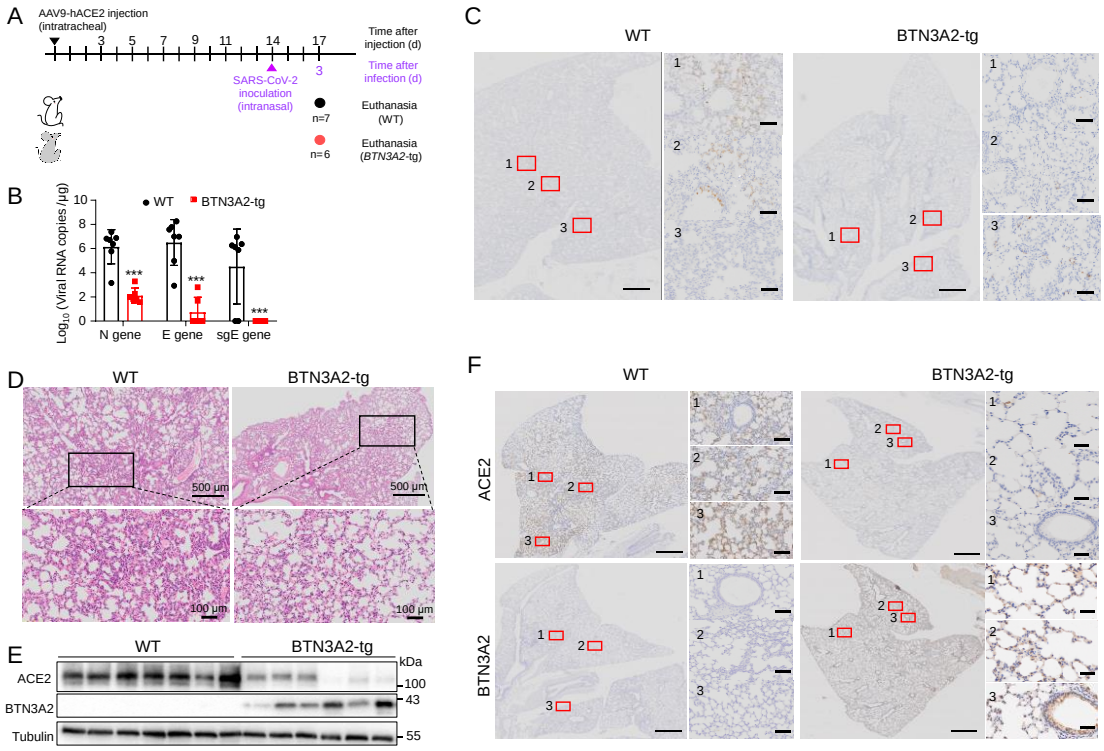

Fig. 6. BTN3A2 suppressed ACE-mediated SARS-CoV-2 entry

A: Schematic of animal experiments with SARS-CoV-2 inoculation. BTN3A2-tg and WT mice were intranasally infected with AAV9-hACE2 (2×10^{12} viral genome copies) for 14 days, with all animals then infected with SARS-CoV-2 variant BA.2 (5×10^{4} $TCID_{50}$). All mice were euthanized at 3 dpi for tissue collection.

B: Viral RNA copies in lung tissues of SARS-CoV-2-infected mice at 3 dpi. Each dot indicates log copies of viral genomic N gene, E gene, and subgenomic E (sgE) of a mixed sample of five lung lobes from an individual mouse. Viral copies are presented as mean±SD. All data are presented as mean±SD. **, $P<0.01$; ***, $P<0.001$; one-way ANOVA.

C: Immunohistochemical analysis of SARS-CoV-2 N protein in lung tissues of WT and BTN3A2-tg mice at 3 dpi. Scale bars: 500 μm for entire lung lobe section (*left*) and 100 μm for enlarged view of boxed areas labeled by numbers in entire section

(*right*).

D: H&E staining of lung sections in SARS-CoV-2-infected WT and BTN3A2-tg mice.

E: AAV-mediated hACE2 expression in lungs tissues of WT (C57BL/6J, *n*=7) and BTN3A2-tg mice (*n*=6) at 3 dpi.

F: Immunohistochemical staining for ACE2 and BTN3A2 in lung tissues of WT and BTN3A2-tg mice at 3 dpi. Scale bars are the same as those in (C).